Marta Chaves Silva

Licenciada em Química Aplicada

Development of multifunctional composite aerosols for lung cancer therapy

Dissertação para obtenção do Grau de Mestre em Química Bioorgânica

Orientador: Prof. Doutora Ana Aguiar-Ricardo, FCT-UNL
Co-orientador: Prof. Doutor Carlos Lodeiro Espiño, FCT-UNL

Júri: Prof. Doutora Ana Aguiar-Ricardo
Presidente: Prof. Doutor Jorge Parola
Arguente: Doutora Ana Vidal Nunes

FACULDADE DE CIÊNCIAS E TECNOLOGIA
UNIVERSIDADE NOVA DE LISBOA

Julho 2016

Development of multifunctional composite aerosols for lung cancer therapy

Dedico esta tese aos meus pais, por todo o apoio incondicional que me deram, e à Sofia pela amizade e ajuda ao longo destes anos…

Agradecimentos

To begin with, I would like to express my gratitude to the financial support from Fundação para a Ciência e a Tecnologia (FC&T) and COMPETE, through the projects UID/QUI/50006/2013 (LAQV) and PhD grants SFRH/BD/51584/ 2011 (A.S.S.). Thanks to PROTEOMASS Scientific Society (Portugal) and to the Unidade de Ciências Biomoleculares Aplicadas-UCIBIO@REQUIMTE (FCT/MEC-UID/Multi/04378/2013) co-financed by the ERDF under the PT2020 for funding support. To Dr. Isabel Nogueira for the SEM images, Nuno Costa for the XRD and BET assays and the NMR group where the NMR spectrometers are part of The National NMR Facility, supported by Fundação para a Ciência e a Tecnologia (RECI/BBB-BQB/0230/2012).

To my professors, Dr. Ana Aguiar-Ricardo and Dr. Carlos Lodeiro, thank you for all the help you have given me, for the opportunity of letting me work within your groups and for the opportunity of letting me present my work in international congresses. I will never forget all the efforts you did to help me.

To Dr. Teresa Casimiro, thank you for all the work advices and for always be available to help me with all my questions, even the existential ones.

To professor Capelo, thank you for all the help and also thank you for giving me the opportunity of presenting my work in your congresses.

To all of my colleagues in the lab 510: Vanessa Almeida, Patrícia Morgado, Gosia Zakrzewska, Ana Inês Paninho, Alexandre Ventura, Dr. Ana Nunes, Dr. Gonçalo Carreira and Catarina Melo; and all the people from lab 308: Dr. Elisabete Oliveira, Jamila Jafari, Adrián Lodeiro and Joana Coelho. I would also like to thank you Mrs. Maria José Carapinha, Mrs. Conceição and Mrs. Idalina for all the help and assistance.

To Dr. Javier Fernandéz-Lodeiro, I don't even know how to thank you. Beside all of the help through all the process of the synthesis of the nanoparticles, you also taught me a lot about science and nanotechnology and always with lot of passion in every word. Thank you!

To Sara Correia and Fabiana Gonçalves… My "gurias"! Seriously, thank you. You have helped through all the difficulties during this thesis, either academic or professional. You will always be in my heart, no matter how different our paths will be.

To Rita Pires, my academic godmother, thank you for all the teachings, all the support and all the hours you spent listening to me procrastinating. I have to thank you a lot!! And I am sure that this friendship will continue until we die.

To Raquel Viveiros, thank you for all the advices and for never let me doubt of myself. For all the talks during lunch and for all the laughs I gave because of your amazing sense of humor.

To all of my friends, who have always been by my side and have always supported me no matter how, even when I was down and away from the world. Thank you for always giving me the right words in the right times and for all of your friendship. Without you none of this would be possible. Thank you Vanessa, Sara, Mariana, Mani, Nádia, Inês R., Rita L., Rita C.,

Inês D., Joana S., Joana P., Inês S., Gonçalo, Carlos, Rafa, Kiki and especially Fábio for never letting me doubt of myself. You are the best friends I could have asked for.

To one of the people who helped me the most, and that has always accompanied me through this entire process and through all my existential issues, my dramas, and my doubts. I can almost call her a sister, a best friend… Thank you for everything Sofia Silva, thank you from the bottom of my heart. I think I will have to keep thanking you for the rest of my life, for real. And also, I could not forget to also thank Dário and Lulu, thank you guys. ☺

And to conclude, I have a final thank you note. To the most important people of my life: to my family, my parents, my grandfathers and my godfather and godmother. Honestly, you are the best, and without you I would have never been able of doing anything of this. Thank you for all the love and unconditional support. I love you from the bottom of my heart!!

Abstract

Lung cancer is the most common type of cancer worldwide with an exponential growth every year. Besides the lately diagnose, lung cancer treatments are often limited to chemotherapy and radiotherapy, both presenting devastating side effects for the patient. Therefore there is a need of developing new ways to fight this problem. Nanotechnology and pulmonary delivery have been combined in order to develop pulmonary drug delivery systems that are able to reach the deep lung and release a drug into lung cancer cells.

Herein we present a new strategy based on the synthesis of strawberry-like gold-coated magnetic nanoparticles (Fe@Au NPs) that are later conjugated with micronization technologies in order to produce respirable dry powders, nano-in-micro formulations. Once surface modifications can be easily made by coating the nanoparticle with a fluorescent polymer, the functionalization of these Fe@Au NPs in aqueous media is proposed using a fluorescent oligomer oligo(2-ethyl-2-oxazoline) endcapped with cysteamine. Fe@Au nanoparticles functionalized with this new class of oligomers (OOxs), synthetized in supercritical carbon dioxide ($scCO_2$), were micronized into polymeric powders in order to produce respirable powders that are able to reach the deep lungs. Once in the lung epithelia, the chosen biodegradable and biocompatible carrier, chitosan (CHT) is expected to release the nanoformulations in a controlled and sustained manner. The micronization process was achieved using sustainable methodologies that also make use of $scCO_2$, the Supercritical Assisted Spray Drying (SASD). The co-atomization of a casting solution with CHT and the produced nanoparticles enabled the production of dry powders with suitable features for pulmonary delivery. The ability of the engineered nanosystems to degrade and release its encapsulated contents was addressed by co-encapsulating the nanoparticles with a model drug (ibuprofen). The optimal conditions for the production of the dry powders were carefully selected by performing a design of experiment (DoE). With the best conditions chosen, two assays were made, one containing the nanoparticles and CHT, and the other containing the nanoparticles, ibuprofen and CHT. Aerodynamic, morphological and physical-chemical characterizations were assessed. Nanoparticles with diameters ranging from 50-200 nm and microparticles with diameters of approximately 3 µm were obtained. The produced dry powders showed great aerodynamic properties, with fine particle fraction values around 60% and mass median aerodynamic diameters around 1.5 µm. An 80% of drug release was achieved after 48 hours of study. These preliminary results show that these nano-in-micro formulations could be potential systems to address pulmonary administration of magnetic nanoparticles.

Keywords: lung cancer, dry powders, supercritical carbon dioxide, nanoparticles, microparticles, supercritical assisted spray-drying, ibuprofen

Resumo

O cancro do pulmão é o cancro mais comum a nível mundial com um crescimento exponencial todos os anos. Para além do diagnóstico tardio, os tratamentos para o cancro do pulmão são frequentemente limitados à quimioterapia e radioterapia, ambos com efeitos secundários devastadores para o paciente. Como tal, há uma necessidade de desenvolver novas formas de combater este problema. A nanotecnologia e a administração pulmonar têm vindo a ser combinadas de maneira a desenvolver sistemas de administração pulmonar de fármacos capazes de alcançar o pulmão profundo e libertar o fármaco para as células cancerígenas.

Aqui, apresentamos uma nova estratégia que tem por base a síntese de nanopartículas magnéticas tipo morangos, parcialmente revestidas com ouro (Fe@Au NPs) que serão, mais tarde, conjugadas com tecnologias de atomização de maneira a produzir pós secos respiráveis: as formulações nano-em-micro. Uma vez que facilmente se pode funcionalizar a superfície das nanopartículas Fe@Au NPs em meio aquoso, estas foram revestidas com um polímero fluorescente, neste caso um oligómero, oligo(2-etil-2-oxazolina) terminado com cisteamina. As Fe@Au NPs funcionalizadas com esta nova classe de oligómeros (OOxs), previamente sintetizados em dióxido de carbono supercrítico ($scCO_2$), foram de seguida atomizadas e simultaneamente encapsuladas numa matriz de quitosano (CHT) de maneira a produzir pós respiráveis capazes de alcançar a zona alveolar do pulmão. Uma vez no epitélio pulmonar, espera-se que o veículo biodegradável e biocompatível escolhido, CHT, liberte as nanoformulações de uma maneira controlada e continuada. O processo de atomização foi conseguido usando metodologias sustentáveis que também fazem uso do $scCO_2$, a Secagem por Pulverização Assistida por CO_2 Supercrítico. A co-atomização de uma solução modelo com CHT e as NPs produzidas permitiram a produção de pós secos com características adequadas à administração pulmonar. A capacidade de os nanosistemas produzidos se conseguirem degradar e libertar os conteúdos neles encapsulados, foi estudada ao co-encapsular as nanopartículas com um fármaco modelo (ibuprofeno). As condições ideais para a produção dos pós secos foram cuidadosamente escolhidas ao realizar um desenho de experiências (DoE). Com as melhores condições escolhidas, dois ensaios foram realizados, um contendo as nanopartículas e o CHT, e outro contendo as nanopartículas, o ibuprofeno e o CHT. Os pós produzidos foram caracterizados em detalhe em termos da morfologia, propriedades físico-químicas e desempenho aerodinâmico. As nanopartículas apresentaram diâmetros entre os 50-200 nm e as micropartículas diâmetros de aproximadamente 3 µm. Os pós secos produzidos mostraram boas propriedades aerodinâmicas, com cerca de 60% de partículas finas e diâmetros aerodinâmicos médios de 1.5 µm. Verificou-se que 80% do fármaco se libertou ao fim de 48 horas de estudo. Estes resultados preliminares mostram que estas formulações nano-em-micro podem ser sistemas potenciais para usar na administração pulmonar de nanopartículas magnéticas.

Keywords: cancro do pulmão, pós secos, dióxido de carbono supercrítico, nanopartículas, micropartículas, *spray-drying* assistido por fluidos supercríticos, ibuprofeno

Table of Contents

ABSTRACT V
RESUMO VII

INTRODUCTION **1**
1.1. DRY POWDER INHALERS 3
1.2. PARTICLE ENGINEERING 4
1.2.1 Supercritical fluids assisted processes *5*
1.2.2. Supercritical assisted spray-drying (SASD) *7*
1.3. NANOPARTICLES AND PULMONARY DELIVERY 10
1.3.1 Strawberry-like nanoparticles *12*
1.3.2. Functionalization of nanoparticles *13*
1.5 CHITOSAN AS AN EXCIPIENT FOR PULMONARY DELIVERY 15
1.9 CHARACTERIZATION OF PARTICLES 17
1.10 WORK THEMATIC 20

EXPERIMENTAL SECTION **23**
2.1 MATERIALS 23
2.2 METHODS 23
2.2.1 Synthesis of the strawberry-like gold coated magnetite nanoparticles *23*
2.2.2 Synthesis of the living oligo(2-oxazoline) *25*
2.2.3 Particle production – SASD apparatus *26*
2.3 PARTICLES CHARACTERIZATION 27
2.3.1 Characterization of nanoparticles *27*
2.3.2 Characterization of microparticles *27*

RESULTS AND DISCUSSION **31**
3.1 NANOPARTICLES CHARACTERIZATION 31
3.2 DESIGN OF EXPERIENCE: CHT AND CHT_IBUPROFEN 34
3. 3 CHARACTERIZATION OF THE CHT_FE@AU_OETOX-SH PARTICLES 45
3.4 CHARACTERIZATION OF CHT_FE@AU_OETOXSH_IBP PARTICLES 52

CONCLUSIONS **59**

REFERENCES **62**

APPENDIX **69**

Index of Figures

Figure 1.1. Example of different inhalers a) DPI; b) nebulizer; c) pDMI 3
Figure 1.2 Schematic representation of (a) a person using an inhaler and (b) a dry powder inhaler 4
Figure 1.3 . Phase diagram of CO2, adapted from M Sihvonen et al.[27] 6
Figure 1.4 Supercritical Assisted Spray-Drying Apparatus used in this work. 8
Figure 1.5 On the right- image of the spray (real representation); on the left – schematic representation of the atomization process combining the two steps of the atomization 9
Figure 1.6 VLE for water-ethanol-CO_2 adapted from C. Duarte et al [34]. scCO_2 conditions: 31.1ºC / 73.8 bar. 10
Figure 1.7 Schematic representation of the production of the final nanoparticle 15
Figure 1.8 CHTstructure, where DA is the degree of N-acetylation Adapted from M. Dash et al. [76] and J. Kumirska et al. [79] 16
Figure 1.9 Collection plates and their corresponding cut-off diameter (μm)for an Anderson Cascade Impactor with an air flow rate of 60 L/min at a pressure drop of 4 kPa .A – schematic representation of an ACI and B – schematic representation seen from inside 18
Figure 1.10 Schematic representation of the mechanism of action of this system 21
Figure 3.11 Zeta potential of the different layers, where the 4[TH] layer corresponds to the final nanoparticles 32
Figure 3.12 Transmission Electron Microscopy images of strawberry Fe/Au nanomaterial functionalized with oligo(2-ethyl-2-oxazoline)s in different magnifications. A and B – magnetite nanoparticles; C, D, E, F and G – Strawberry-like gold magnetite nanoparticles functionalized with oligo(2-oxazoline) 33
Figure 3.13 Fluorescence vs Absorbance of the final nanoparticles. The emission band can be denoted at 384 nm (orange line) and the absorption band can be seen at 300 nm (blue line). 34
Figure 3.14 Design of Experiment for CHT and CHT_IBP assays 35
Figure 3.15 Representation of the distribution of CHT powders through the different stages of the ACI 39
Figure 3.16 Morphologi G3 images of the produced CHT powders 40
Figure 3.17 Representation of the distribution of CHT_IBP powders through the different stages of the ACI 43
Figure 3.18 Morphologi G3 images of CHT_IBP powders 44
Figure 3.19 Morphologi G3 images of CHT_Fe@Au_OEtOx-SH powders at different magnifications: a) 5x, b) 10x, c) 20x, d) 50x. 46
Figure 3.20 SEM images of A and B – CHT; C and D – CHT_Fe@Au_OEtOx-SH 47
Figure 3. 21 Representation of the particles distribution (with and without a magnet) troughout the different stages of the ACI. I.p stands for induction port. 48
Figure 3.22 Representation of particles distribution throughout the different stages of the ACI 49

FIGURE 3.23 FT-IR SPECTRA OF THE NANOPARTICLES AND CHT FORMULATIONS 50
FIGURE 3.24 XRD PATTERN OF CHT AND CHT_FE@AU_OETOX_SH.....51
FIGURE 3. 25 - RELEASE STUDY OF THE NANOPARTICLES FROM THE MICROPARTICLES USING A MAGNET. FIGURE ON THE LEFT SHOWS THE FLASKS CONTAINING THE POWDERS IN DIFFERENT PH SOLUTIONS.....52
FIGURE 3. 26 MORPHOLOGI G3 IMAGES OF CHT_FE@AU_OETOX-SH_IBP FORMULATIONS 53
FIGURE 3.27 REPRESENTATION OF PARTICLE DISTRIBUTION THROUGHOUT THE DIFFERENT STAGES OF THE ACI.....55
FIGURE 3.28 A) *IN VITRO* CUMULATIVE RELEASE STUDIES AT DIFFERENT PHS; B) KORSMEYER-PEPPAS ADJUSTMENT FOR 60% OF THE RELEASE 56
FIGURE 4.29 SCHEMATIC REPRESENTATION OF THE DELIVERY OF A DRY POWDER CONTAIN MAGNETIC NANOPARTICLES IN ORDER TO GUIDE THEM TO THE DESIRED REGION(S) OF THE LUNG BY USING OF A STRONG EXTERNAL MAGNETIC FIELD. ADAPTED FROM M. DOLOVICH ET AL. [105] 60
FIGURE A30 ABSORBANCE AT DIFERENTE CONCENTRATIONS OF THE POLYMER.....69
FIGURE A31 CALIBRATION CURVE OF THE POLYMER 70
FIGURE A32 POLYMER INTENSITIES AT DIFERENTE CONCENTRATIONS.....70
FIGURE A33 CALIBRATION CURVE AT DIFFERENT POLYMER CONCENTRATIONS.....71
FIGURE A34 ^{1}H NMR SPECTRUM OF THE POLYMER 72
FIGURE A35 ^{13}C SPECTRUM OF THE POLYMER 73

Index of Tables

TABLE 3.1 OPERATING CONDITIONS FOR DOE CHT ASSAYS 36
TABLE 3.2 AERODYNAMIC PROPERTIES OF CHT DRY POWDERS AND YIELD 37
TABLE 3.3 MORPHOLOGI G3 RESULTS FOR THE PRODUCED CHT POWDERS 38
TABLE 3.4 OPERATING CONDITIONS FOR DOE CHT_IBP ASSAYS.....41
TABLE 3.5 AERODYNAMIC PROPERTIES OF THE PRODUCED CHT_IBP POWDERS 42
TABLE 3.6 MORPHOLOGI G3 RESULTS FOR THE PRODUCED CHT_IBP POWDERS.....43
TABLE 3.7 MOISTURE CONTENT AND MORPHOLOGICAL CHATACTERIZATION OF ASSAY 5 FROM BOTH CHT AND CHT_IBP.....45
TABLE 3.8 – POWDERS PHYSICAL CHARACTERISTICS. ND – NOT DETECTABLE. 45
TABLE 3.9 AERODYNAMIC PROPERTIES OF CHT_FE@AU_OETOX-SH POWDERS USING A MAGNET AND WITHOUT USING A MAGNET 47
TABLE 3.10 AERODYNAMIC PROPERTIES OF CHT AND CHT_FE@AU_OETOX-SH FORMULATIONS. ..49
TABLE 3.11 PHYSICAL PROPERTIES OF CHT_FE@AU_OETOXSH_IBP PARTICLES.....53
TABLE 3.12 AERODYNAMIC PROPERTIES OF CHT_FE@AU_OETOX-SH_IBP FORMULATION.....54
TABLE 3.13 KORSMEYER-PEPPAS ADJUSTMENT VALUES FOR IBP RELEASE 56
TABLE 3.14 ABSORBANCES AND CONCENTRATIONS OF THE DRUG RELEASE STUDY AT PH 6.4.....75
TABLE 3.15 ABORBANCES AND CONCENTRATIONS OF THE DRUG RELASE STUDY AT PH 7.4 76

Abbreviations

CHT – Chitosan

IBP – Ibuprofen

NP – Nanoparticle

Fe@Au_NP – Strawberry-like gold-coated magnetite nanoparticles

MMAD – Mass Median Aerodynamic Diameter

FPF – Fine Particle Fraction

RF – Respirable Fraction

GSD – Geometric Standard Deviation

EF – Emitted Fraction

EE – Entrapment Efficiency

OETOx – Oligo Ethyl Oxazoline

DPI – Dry Powder Inhaler

$\mathbf{D_{v,50}}$ – mean volume diameter

$\mathbf{D_{v,90}}$ – volume diameter at 90% of the population

$\mathbf{D_{v,10}}$ – volume diameter at 10% of the population

1

Introduction

Lung diseases are one of the most common medical conditions throughout the world. Either caused by environmental pollution, smoking or genetics, lung diseases, such as asthma, chronic obstructive pulmonary disease (COPD), chronic bronchitis, cystic fibrosis and lung cancer, can have a tremendous impact on peoples' health leading, most of the times, to death.[1,2] To address these conditions, different systems that can easily carry active drugs into the site of action and thus initiate the respective treatments, have been widely investigated.[2] A suitable drug carrier or drug delivery system (DDS) should protect the drug against degradation, ensuring that the drug attains suitable permeability properties and it is carried to the desire site of action. [3]Therefore, the treatment efficacy mostly depends on the techniques by which the drug is delivered (carrier and administration route) and optimum concentration of the drug, above or below this range can be toxic or produce no therapeutic effect at all.[4,5] Hence, besides choosing an adequate carrier, it is off extremely importance to decide on an adequate route of administration. Due to its simplicity, convenience, and patient acceptance, oral administration is the most common and preferred drug delivery route. However, this route has a risk of drug decomposition by the digestive system, resulting in poor and ineffective drug bioavailability. Transdermal drug administration is also simple and easy to perform; however drug adsorption is typically inefficient. On the other hand, intravenous (IV) administration results in high adsorption efficiency, which may lead to a toxic blood level after injection and sometimes, an under concentration on the desired threshold towards the end of the dosing interval. Moreover, it is an invasive method that can create pain at injection sites.[4,6] In an attempt to circumvent the problems faced by the above-mentioned routes, pulmonary administration has been widely investigated once it enables the targeting directly to the lung for both local and systemic treatment.[5,7] In fact, lungs have been widely investigated since the ancient times as a route for drug delivery. Egyptians, for instance, used to inhale vapors for the treatment of different diseases (1500 BC), and in the middle

1920s aqueous nebulizers were used for the treatment of lung infections. However, the use of this specific route was forgotten until the year of 1956 with the invention of the first metered dose inhaler (MDI) used in the delivery of albuterol for asthma treatment.[1,2] There has been some developments in this area and dry powder inhalers (DPIs) appeared as an alternative to MDI. Since then, pulmonary drug delivery has suffered major advances as an alternative to other routes.[8]

Due to their large surface area, easily permeable membrane, thin absorption membrane (0.1 - 0.2 μm), elevated blood flow (5 L/min), thin alveolar epithelium and extensive vascularized alveolar epithelium offering a large absorptive surface (80 – 100 m^2), lungs can easily and rapidly absorb soluble and permeable active compounds.

Moreover, local treatment is advantageous once there is low enzymatic activity, relatively low local metabolic activity and the drug avoids the first-pass metabolism and is directly carried into the site of action.[9] Pulmonary delivery together with controlled release systems enables drug protection from rapid degradation or clearance; enhances the accumulation in the cells by increasing its bioavailability, therefore lowering the amount of drug required, reducing harmful side effects and reducing costs.[2,10–12] However, there are some disadvantages of pulmonary administration being the most common one the short duration of drug action. Therefore, it is necessary to develop controlled release systems for pulmonary administration that enable the drug in a controlled and sustained manner to the site of action and therefore obtain a more controlled drug action.

Polymeric microparticles have been used as drug carriers for controlled delivery systems. These microparticles were usually regarded simply as carriers and they were not expected to have any special features besides their suitable sizes for inhalation and dryness. Recently, with the wide investigation in the inhalation field, particles' requirements became more complex and the systems should be carefully designed in order to perform specific functions such as the transport of the drug, targeted delivery, sustained drug release and drug stabilization.[13–15]

The inhalation technology can be divided into two main areas: i) the development of inhalation devices, through the design of more sophisticated inhalers (though they are complex and expensive); and ii) particle engineering, a discipline that assembles the knowledge from different areas, such as chemistry, solid state physics, aerosol and powder science. This concept is used in the design of particles with suitable characteristics for the different needs of the patients.[16]

1.1. Dry powder inhalers

A good inhaler device should generate an aerosol of a suitable size (1-5 μm), with a reproducible drug dosing ensuring that both chemical stability and activity of the drug are maintained intact. Also, the device should be simple, easy to use, inexpensive and portable. Nebulizers, where the drug is dissolved in a polar liquid, were the first inhalers to be developed and to appear in the market. Since they were not portable, their use was confined to hospitals and homes. Along with this, they also showed some disadvantages, such as low efficiency and reproducibility.[2,3,11] Pressurized metered dose inhalers (pMDIs) were developed in order to overcome these disadvantages. These new devices not only showed a greater efficiency and reproducibility, but they were also easier and faster to use and portable. However, they required the use of compressed volatile liquids as propellants, (i.e. chlorofluorocarbon and hydrofluoroalkanes), making them environmentally unfriendly and since they deliver the dose at high velocity it facilitates the deposition in the oropharynx, which induces local and systemic side effects.[17] Dry powder inhalers (DPIs) appear in order to overcome all these problems. Examples of different inhalers are given in Figure 1.1.

Figure 1.1 Example of different inhalers a) DPI; b) nebulizer; c) pDMI

DPIs are also easy to use and portable; however unlike pMDIs they are propellant-free, making them environmentally friendly. In this case, the aerosols are in a dry state, assuring the stability of the drug, therefore there is no need of special storage conditions and distribution. However, DPIs are expensive and complex to develop. Most of them have a minimum inspiratory effort that is needed for proper use, thus insufficient patient inhalation flow rates may lead to reduced dose delivery and incomplete disaggregation of the powder, leading to unsatisfactory device performance and subsequently for the break-up of the powder into smaller particles in order to reach the deep lungs, for this reason such DPIs are normally used only in older children and adults.[18,19] Nonetheless, if handled correctly the pharmaceutical products used in DPI may result in high local levels of drug in epithelium flu-

ids of the airways and lower respiratory tract. [12,18,20,21] DPIs can be classified as “single-dose” devices, which use a single dose capsule; in “multiple unit dose” DPIs, which contains small doses separated in several capsules or blisters; and in “multidose” DPIs that contains an amount of powder that is then delivered in several metered doses.[21] A schematic representation of a person using a DPI is given in Figure 1.2.

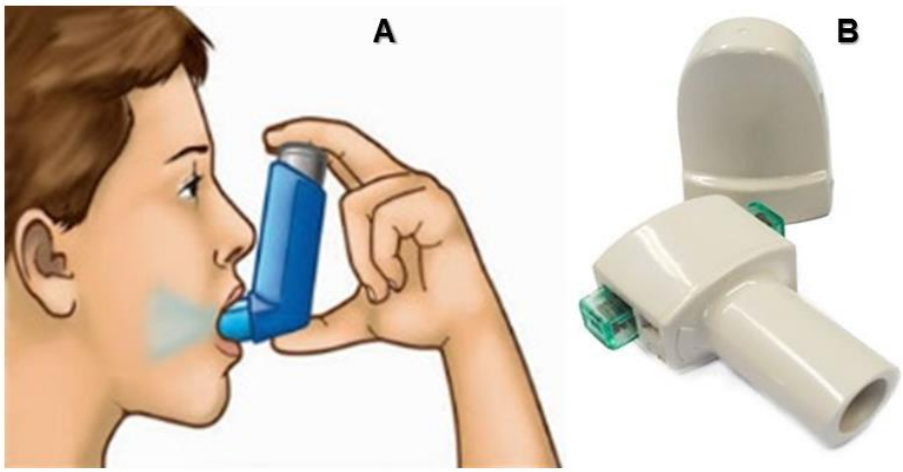

Figure 1.2 Schematic representation of (a) a person using an inhaler and (b) a dry powder inhaler

1.2. Particle engineering

There are several different processes for the production of particles. Among these we can find milling, spray-drying (SD), spray freeze-drying (SFD) and supercritical fluid assisted processes.[22] Due to the vast thematic regarding the last process, supercritical fluid assisted processes are detailed in a subcategory.

Milling is a method of drug powder micronization and most of the inhalation powders are prepared with a jet mill. This process involves micronization by interparticle collision and attrition. In sum, the gas passes through a nozzle and particles go into the jet mill where they are fractured into smaller ones (while in the gas stream) due to interparticle collisions. The path taken by the gas stream allows the exit of fine particles while the larger ones remain in the jet mill for further micronization. However, jet milling has lack of control over parameters such as size, shape, morphology and surface properties and most of the times, due to the high energy required; crystal surfaces are damaged resulting in chemical and physical instability of the drug.[16,23]

SD is a process that forces a fluid through a nozzle, producing a mist that is dried to produce a fine powder. The technique employs a variety of different types of nozzles, some of which use ultrasound or air-jet shear to nebulize drug suspensions. SD is very rapid, convenient and has very few processing parameters, making it suitable for industrial scalable processing and it also provides stability and biological activity for the active pharmaceutical ingredient (API). In this process, drug/protein/peptide loaded microspheres are prepared by the means of an atomization of the feed solution into a spray, which later enters in contact with heated air in a drying chamber forming a dry powder. The nature of the used solvent, temperature of the solvent evaporation and feed rate affect the morphology of the microspheres. Unfortunately, this process often utilizes co-solvents to improve drying and/or large amounts of excipient to stabilize the drug and to maintain powder properties. Also, there is a low adhesion of the microparticles to the inner walls of the spray-dryer, turning the yields insufficient, and the possible degradation of heat-sensitive drugs.[16,19,24]

SPF consists on spraying a solution into a vessel containing a cryogenic liquid such as nitrogen, oxygen or argon where the droplets are quickly frozen. Then, these frozen droplets are lyophilized resulting in porous spherical particle suitable for inhalation. Yet, there are some disadvantages associated with this process, such as the degradation of the products from the freezing and drying steps. Like spray drying, loss of stability and aggregation remains a major challenge.[16,24]

1.2.1 Supercritical fluids assisted processes

Supercritical fluids (SF) are compressed gases or liquids above their critical temperature and pressure but below the pressure required for solidification to occur. It provides adjustable solvent properties based on temperature and pressure and also the possibility of operating at mild conditions with reduced use of organic solvents, making this technology an alternative to conventional methods for pharmaceutical manufacturing. SFs are widely used since they have the density of a liquid, which shows advantageous solvation power, and they also have the viscosity of a gas, which confers them a high diffusivity. Since these aspects are very changeable near the critical point, it is easy to control both of them by a slightly change in pressure/temperature. Also, near the critical point the compressibility and the heat capacity are much higher than in other conditions.[25,26]

The most used SF is carbon dioxide (CO_2), since it is nontoxic, nonflammable, has a low cost and is readily available in high purity from a variety of sources. This happens since CO_2 is a subproduct of the industry that can be easily captured and used for other ends. One of the main reasons of using CO_2 is that, during any process it is possible to separate the solvents and residues from the final product by simply reducing the pressure of the system,

since CO_2 is a gas at normal temperature and pressure, leading to highly pure materials. Also, it has a low critical point (31.1°C / 73.8 bar)[27] (Figure 1.3), which is suitable to use with heat-sensitive materials and can reduce manufacturing complexity and energy. The only constraint facing the use of supercritical carbon dioxide ($scCO_2$) is its limited solvation power to polar substances. However, such limitation can be turned into an advantage in a situation where it is used as an anti-solvent. Nevertheless, it is possible to modify the solvation power by incorporating a small amount of a volatile compound, such as acetone or ethanol.[27,28]

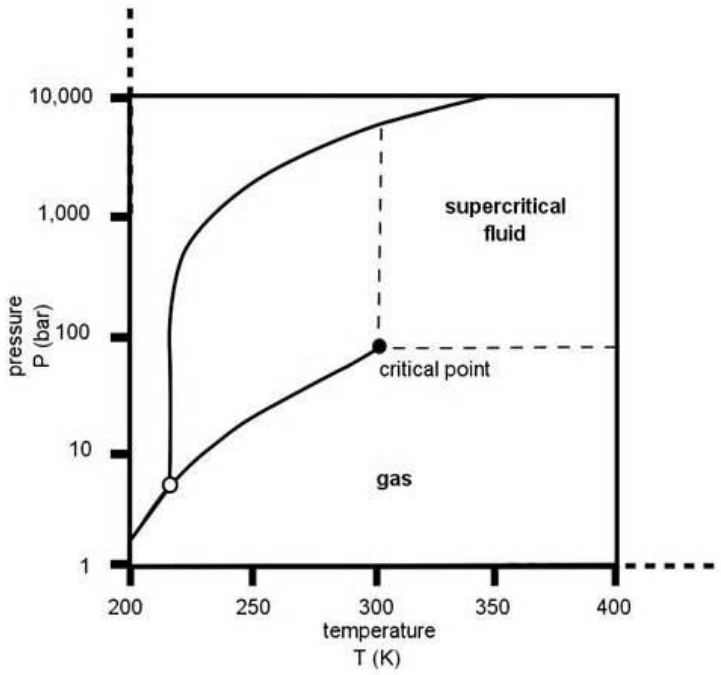

Figure 1.3 Phase diagram of CO_2, adapted from M Sihvonen et al.[27]

As stated above, the conventional techniques such as spray-drying have some limitations, especially in the removal of organic solvents. In order to overcome some of these problems, alternative particle production methods using SFs, especially $scCO_2$, have been proposed.[27] When using $scCO_2$ the use of organic solvents can be minimized or eliminated. This happens due to $scCO_2$ high affinity for those solvents, which enables their removal. A rapid expansion of the CO_2 using a pressure drop leads to the clustering of CO_2 molecules inside the liquid polymer, expanding it and inducing pore formation, making the system suitable for drug deliver. Moreover, changing operating parameters such as pressure, temperature and gas release rate can easily alter the morphology and porosity. By changing these parameters, we are able to control pore size in the final powders, an important feature that increases particles flowability in the respiratory tract.[16,26,29]

SFs have been widely used in particle engineering and it can be divided into three methods: precipitation from supercritical solutions composed of SF and solutions; precipitation from gas saturated solutions; and precipitation from saturated solids using SF as anti-solvent. The first method is based on the solubilization of a drug into $scCO_2$ followed by the rapid expansion of the SF solution into a heated hole, causing the reduction of the solution density, and therefore decreasing the solvation power of the SF. This will lead to the precipitation of the drug and the process is denominated *Rapid Expansion of Supercritical Solution* (RESS). The second method is similar to the first one since they both involve $scCO_2$ as a solvent. However, in this specific process, $scCO_2$ is used as a co-solute and is dissolved in a melted solute and the resulting SF solution is fed via an orifice into a chamber, leading to a rapid expansion under normal pressure and temperature conditions.[18,22] This method has been called *Precipitation from Gas-Saturated Solution* (PGSS). The last method is the most common one and makes use of the high solubility of $scCO_2$ in organic solvents, which leads to a volume expansion when the fluids make contact. Thus, there is a reduction in solvent density and in the solvation capacity. Such reduction causes increased level of supersaturation, solute nucleation and particles formation. This method has been assigned different names such as *Gaseous Anti-solven*t (GAS), *Aerosol Solvent Extraction System* (ASES), *Solution Enhanced Dispersion by SF* (SEDS) and *Precipitation by Compressed Anti-solvent* (PCA).[19,22]

Recently, Supercritical Fluid Assisted Atomization (SAA) has gained some recognition since it shows more advantages over other methods like the ones referred above. This process was first described by G. Della Porta et al. [28] where supercritical CO_2 and a solution of a drug (in water or organic solvent) are mixed together and sprayed into a chamber at near atmospheric pressure conditions. Then a heated flow of nitrogen enters the chamber to dry the particles.[26,30] In the next subcategory a more detailed explanation is made.

1.2.2. Supercritical assisted spray-drying (SASD)

Supercritical Assisted Spray-Drying (SASD) is a process similar to the one patented by E. Reverchon in US 7276190B2 under the name *Process for the production of micro and/or nano particles,* and is based on the solubilization of controlled quantities of $scCO_2$ in liquid solutions. SASD is, in fact, a supercritical assisted atomization, referred in the last subcategory, however some conditions were optimized.[31] The SASD apparatus (Figure 1.4) consists in two pumps: one to deliver the liquid solution and another one to deliver the liquid; a saturator – the static mixer; a precipitator; a cyclone; and a glass flask. The pumps are used to deliver both solutions to the saturator. Since the CO_2 pump only pumps liquid solutions, CO_2 must be liquefied. Therefore it passes through a cryostat and is then heated above its critical temperature. Once it reaches the saturator, the pressure is raised until su-

percritical conditions. The mixing takes place in static-mixer containing high-surface packing that ensures long residence times in order to achieve near-equilibrium conditions.[32]

Figure 1.4 Supercritical Assisted Spray-Drying Apparatus used in this work (real life picture).

Once all the conditions are met, the solution is expanded through a nozzle (with a 150.µm diameter) and is atomized by a two-step atomization: the first primary droplets are obtained due to pneumatic atomization when exiting the nozzle; then a secondary atomization process takes place by decompressive atomization due to CO_2 expansion from inside the primary droplets, shown in Figure 1.5. This implies that the smallest particle size that can be achieved is the size of the smallest droplet achieved during the first atomization. The droplet size is determined by viscosity, surface tension and the amount of $scCO_2$ dissolved in the liquid solution, while temperature and chemical characteristics of the solute determine whether the particles are crystalline or amorphous. SASD offers many advantages over conventional methods, the possibility of operating in a continuous method in mild operating conditions and the ability of using both organic and inorganic solvents while at the same time providing a good control over particle size and distribution.[26,32]

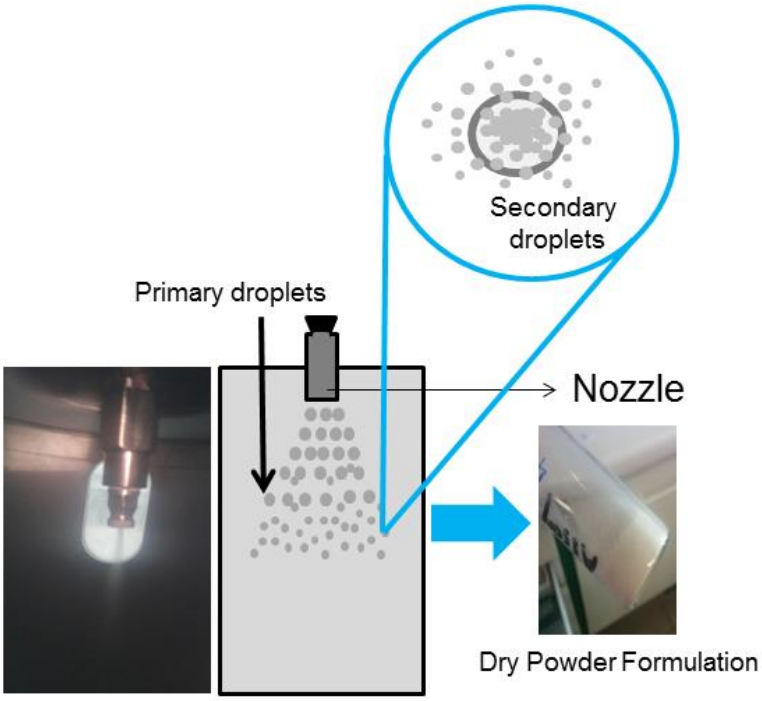

Figure 1.5 On the right- image of the spray (real representation); on the left – schematic representation of the atomization process combining the two steps of the atomization

SASD process performance is strictly related to the CO_2 solubilization in the liquid solution, which dictates the efficiency of the atomization process. The amount of CO_2 solubilized depends on the solvent, temperature, pressure and residence time in the static mixer. These parameters are related to high-pressure vapor liquid equilibrium (VLE).[33] In this work, acidic water (1% v/v) and ethanol were the solvents used. The amount of acetic acid in the solution is minimal and there is a lack of information in the literature about the solubility of acetic acid/water mixtures in CO_2, therefore and since there is more information on ethanol-water-CO_2 ternary system, the operating conditions are estimated taking into account the VLE ternary system of ethanol-water-CO_2.[34,35] Nevertheless, acetic acid may have some influence on the VLE, and this should also be taking into consideration. When fixing a determined pressure and temperature, the mass flow ratio between CO_2 and the solvent, we can determine the operating point of the ternary system as depicted in Figure 1.6.

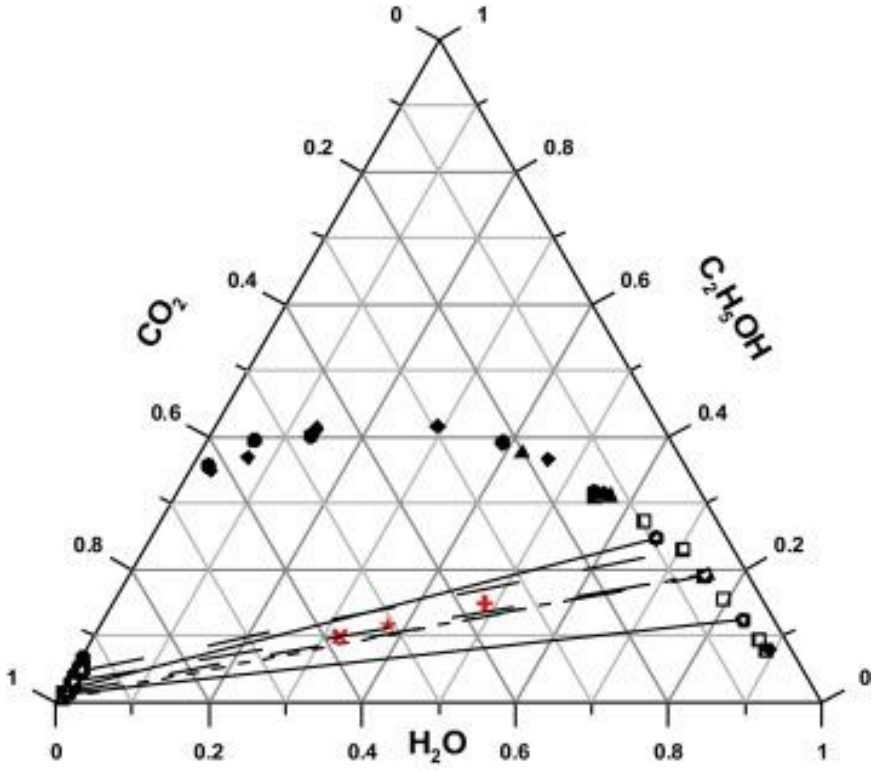

Figure 1.6 VLE for water-ethanol-CO_2 adapted from C. Duarte et al [34]. $scCO_2$ conditions: 31.1ºC / 73.8 bar.

The solubility of CO_2 in aqueous solutions is low when working at relatively low pressures and temperatures since the operating point falls in the region of the two-phase gas liquid. [36] When adding small amounts of ethanol to the solution, and since CO_2 has a higher affinity to non-polar solvents, the miscibility of $scCO_2$ in water can be improved and process efficiency can be increased once the majority of the water mixed with ethanol is taken along with CO_2.[35,37] However, the operating point still falls in a two-phase region, so the gas to liquid ratio is not affected. The solubility of $scCO_2$ is also important once it interferes in particles production: when dissolved, it reduces the viscosity and surface tension of the solution; when non-dissolved, it enhances the pneumatic effect, therefore improving primary atomization.[22,35,37]

Different compounds have already been atomized using SAA technology, such as BSA, aluminum sulfate, sodium chloride, among others. In our group, different pulmonary excipients have also been atomized, for example cholesterol, CHT, PLGA, leucine and lactose.

1.3. Nanoparticles and pulmonary delivery

Size and morphology are two main features to be considered in particles design.[18,19] Porous particles have both large specific surface area and volume diameter, and show better

bioavailability. Moreover, particles targeted to the deep lung, should have a small aerodynamic diameter (d_{ae}) in order to pass through mouth, throat and conducting airways, reach the deep lung and avoid macrophage clearance, but not so small that they can not deposit and therefore be vented. [33,38] Fine particles, the fraction of particles that can reach the lower respiratory tract may adhere to the epithelium membrane and can be cleared more slowly.[7,39,40] Particles with larger specific surface area (with porous and with a large volume diameter) show better flowability. Therefore, respirable particles, i.e., particles to be respirable, should present aerodynamic diameters in a range of 1–5 µm, when dry. Upon contact with an aqueous solution, particles should swell increasing their size and avoiding macrophage clearance in the deep lung, as they also provide a controlled and sustained release of the drug carried out.[39,41,42]

Different systems using microparticles have been investigated, such as microparticles comprised of one polymer, co-polymers or nanoparticles inside microparticles allowing a better control over the drug release.[43,44]

Recently, nanotechnology has been combined with pulmonary delivery as nanoparticles can be used as efficient drug carriers providing a controlled release of the drug entrapped and specifically recognizing cellular types.[44–46] In fact, over the last two decades nanotechnology has been providing extraordinary outcomes in both drug delivery and cell targeting. Thus, the merging of nanotechnology and pulmonary delivery can bring new improvements for the diagnosis and therapy of several types of lung and systemic diseases.[5,47] Due to their small size (1-150 nm), NPs can easily penetrate the deep tissue and be taken up by cells more easily while protecting the drugs at both extracellular and intracellular levels. [48,49] These achievements have been shown to improve drug half-lives and retention, which will substantially decrease unwanted side effects. Besides their therapeutic capabilities, nanoparticles can also be designed to exhibit diagnosis features, thus creating theragnosis nanosystems. Nanoparticles with theragnosis capabilities can offer many benefits for lung disease patients including real time diagnosis, adequate therapy for individual patients (personalized medicine) and reduction of adverse drug effects.[5,47]

In an attempt to produce theragnosis systems, different types of nanoparticles, such as metal (like gold (Au), ferric (Fe) and silver (Ag)) or polymeric, (like Polyethylene-glycol (PEG), silica (Si) and poly(lactic-co-glycolic acid) (PLGA)), have been widely investigated.[50] The majority of metal NPs have proven to be excellent drug carriers. Also, they are, easily functionalized and can be used as active targeting nanocarriers, which is matter of extremely importance.[50,51] NPs lacking functionalization are more likely to interact with plasma proteins or uptake my macrophages. By controlling nanoparticles surface properties a stealth character can be conferred to the nanosystems, preventing agglomeration and opsonization, there-

fore protecting them and thus increasing their residence time and ensure the delivery of the drug to the desired site of action.[50–52]

In order to produce reliable theragnosis nanoparticles to use through pulmonary administration in a lung cancer condition, a specific type of nanoparticles (strawberry nanoparticles), comprising metallic nanosystems such as magnetic and gold nanoparticles, were fully investigated and their features are detailed in the next subsections.

1.3.1 Strawberry-like nanoparticles

Strawberry-like nanoparticles (SLNs) is a designation given to core-shell nanoparticles when the shell is formed by small nanoparticles which are only partially covering the core. [53] This designation is based on the structure and conformation of the nanoparticles because since the core is not entirely covered, it is similar to a strawberry and its seeds. SLNs are interesting since it is possible to obtain a nanoparticle with different characteristics and properties that are conferred from both the core and the shell. This happens because, as the core is not fully covered, some of its properties and features are able to "flow out" through the open areas of the shell and therefore conferring the same characteristics to the whole system.[54] Different types of SLNs can be found, being multifunctional hybrid magnetic nanoparticles (HNPs) constituted of a magnetic core like magnetite (Fe_3O_4) and a metal shell like gold (Au) interesting ones, especially when used for biomedical applications. E. Umut et al, have proven that Au–Fe_3O_4 HNPs have optical activities through Au and can be used as MRI contrast agents, meaning that they can exhibit properties from both the components and therefore be classified as multifunctional materials.[55,56] Another important factor for the use of the gold shell in this system is that since magnetite nanoparticles are not stable and tend to aggregate, the gold shell will confer them some stability, avoiding aggregation, and will confer them more biocompatibility as well.

1.3.1.1 Magnetite nanoparticles

Superparamagnetic molecules are those that are attracted to a magnetic field but do not retain residual magnetism after the field is removed. These nanoparticles are of great interest since they have different and fascinating advantages, such as: they can be visualized in magnetic resonance imaging (MRI) due to their paramagnetic properties; they can be guided to a location by the use of magnetic field and heated by magnetic field to trigger the drug release.[57]

Magnetite nanoparticles are SPIONs (Superparamagnetic Iron Oxide Nanoparticles) that are composed of an iron oxide core. This core can be coated either by inorganic (silica, gold) and organic materials (phospholipids, fatty acids, polysaccharides, peptides or other surfactants and polymers).[58] Magnetite NPs features are based on their inducible magnetiza-

tion and their magnetic properties, which allow them to be directed to a defined location or heated in the presence of an externally applied magnetic field. These features can be applied in separation techniques and contrast enhancing agents for MRI. Also, they can be used as drug delivery systems, for magnetic hyperthermia and magnetically assisted transfection of cells.[59–62] However, naked particles tend to be very unstable over long periods of time and tend to form agglomerates. Therefore, it is important to coat them with a stable material, like gold [63] Moreover and despite their low toxicity, they can also induce cell damage, by forming oxygen reactive species. Some strategies comprising grafting or coating are used in order to prevent this toxicity and the possible aggregation. [63,64]

1.3.1.2 Gold nanoparticles

Gold nanoparticles (AuNPs) have long been used as delivery systems and recent studies have shown the efficiency of this system in lung cancer treatment. [44,50,65] Due to its advantages, AuNPs can be used as a coating agent in the formation of strawberry-like nanoparticles. Therefore, by combining the magnetite core with a gold shell we can obtain magnetic particles with gold nanoparticles features as well – Fe@Au NP.[62]

AuNPs optical probes have many advantages due to their inertness and non-toxic core, great metal stability, ease of synthesis and surface functionalization, monodispersibility and biocompatibility, strong light absorption and scattering effect, high photothermal conversion rate and photostability.[66] However, colloidal AuNPs easily aggregate especially when high salts and certain biological molecules are present. Therefore, the design of functional AuNPs must be handled with care in order to assure their properties and stability. In cancer research, AuNPs have been studied since it is possible to coat them with fluorescent agents capable of targeting to cells and tissues, thus nonspecific toxicity can be minimized and transportation efficiency can be enhanced. [67,68] However, AuNPs are well known to self-quench upon surface fluorescent tagging. Therefore it is necessary to come up with a strategy that is able to confer AuNPs fluorescence and at the same time reducing the self-quenching effect. [50]

1.3.2. Functionalization of nanoparticles

Nanoparticles functionalization provides a stealth surface to prevent opsonization, therefore increasing their residence time and enhancing therapeutics delivery at the precise site of action. Usually, such protection is made by hydrophilic polymers like poly(ethylene glycol) (PEG).[69,70] PEG is the most known and commonly used polymer for conjugation in drug delivery. However, some recent reports state that increasing amounts of PEG may lead to undesired hepatic accumulation leading to an inflammatory response trigger by the

liver.[50,71] Therefore, poly(2-ethyl-2-oxazoline)-based lipid conjugates have been proposed as alternative to PEG-based materials. A. Mero *et al*.[71] reported in their work that the properties of polyoxazolines-conjugates could be compared with those of similar PEG-conjugates.
In this work, oxazoline-based polymers are used once they show relatively non-toxicity and are generally water soluble and biodegradable.[72] This kind of materials have been studied for many different applications such as smart materials, drug carriers, membrane structures, synthetic vectors for DNA and RNA delivery, antimicrobial agents and can also be used for nanoparticles protection due to their versatility and ability to form functional materials.[69,72,73] Cationic ring-opening polymerization (CROP) is used in the preparation of *living* polyoxazolines produced in a controlled manner. The term *living* comes from the fact that at the end of the polymerization, the end of the polymeric chain remains active until it is directly terminated.[74] The synthesis of these oligo(2-oxazoline)s is carried in a high-pressure cell and in $scCO_2$. Here, the monomer (a heterocycle) is placed inside the cell and an initiator is added, and *living* CROP occurs.[73] At the end of the polymerization, and due to incorporation of carbamic acid in the oligomer chain during the reaction with $scCO_2$, the final product displays fluorescent properties under UV light. In the beginning, the propagating specie is an oxonium ion and water must be avoided. Then, once the *living* polymerization occurs, it is terminated by a nucleophilic attack of a heteroatom in the growing polymer chain. In this polymerization the final result is a cyclic oligomer that was terminated in an intramolecular way. Initiators are strong electrophiles like boron trifluoride etherate.[69,74,75] The interest in this class of polymers is increasing due to their particular characteristics and extensive applications in chemistry, biochemistry and pharmacology. [71,74]

Bearing this in mind, in this work oligo(2-oxazoline)s were used to confer nanoparticles fluorescent properties so that they can be tracked using confocal microscopy and to protect them from opsonization and degradation. [50]

In this work, the obtained *living oligomer*, oligo(2-ethyl-2oxazoline) was later end-capped with cysteamine, which covalently attaches to the AuNPs shell through the reaction between gold atoms and the thiol group of the cysteamine (Au-S). The resulting particles were denominated Fe@Au_OEtOx-SH and a scheme illustrating particles formation is given in Figure 1.7.

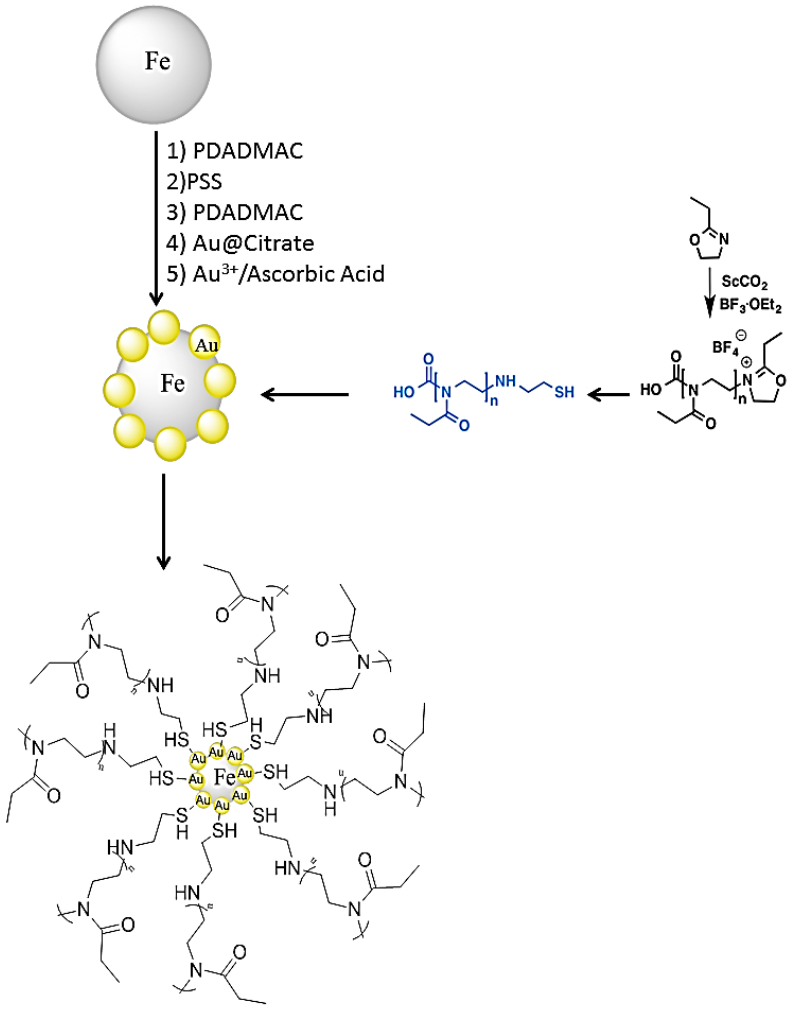

Figure 1.7 Schematic representation of the production of the final nanoparticle

1.5 Chitosan as an excipient for pulmonary delivery

Although the local administration of nanotherapeutics to the lungs may represent the best alternative to improve lung cancer, NPs are not in a size that is suitable for deep lung delivery as they can be easily exhaled and mucociliary cleared out before reaching the underlying epithelium. [50] Therefore the major challenge of pulmonary delivery is to find an adequate carrier system. By using mucoadhesive materials such as CHT it is possible to extend the presence of nanoparticles or drugs in the lung epithelium.[76]

CHT is a cationic linear polysaccharide obtained from the N-deacetylation of chitin (Figure 1.8). It is a co-polymer comprising N-acetyl-2-amino-2-deoxy-D-glucopyranose and 2-amino-2-deoxy-D-glucopyranose. Being the second most occurring polysaccharide in nature, next to cellulose, and being present in crustaceous shells, chitin is easily used without caus-

ing much damage to the environment. Several millions of tons of chitin are harvested each year as the shell waste of crustaceans, making it a relatively cheap and a readily available source.[76,77] Many applications of CHT have been proposed for both therapy and theragnosis, such as for the delivery of therapeutic agents, bioimaging, tissue engineering, wound healing and stimuli-responsive materials.[78]

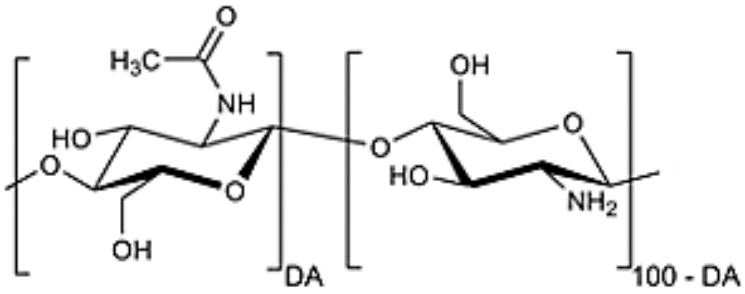

Figure 1.8 CHTstructure, where DA is the degree of N-acetylation Adapted from M. Dash et al. [76] and J. Kumirska et al. [79]

For the delivery of therapeutic agents, CHT has been successfully applied to gene delivery, growth factor hormones, proteins like bovine serum albumin (BSA), and drugs such as ibuprofen, doxorubicin, dopamine and paclitaxel. CHT has already been proved to be biodegradable, biocompatible and non-toxic, thus it is an interesting choice to be used as a drug carrier, protecting the drug against enzymatic degradation. However, some concerns rely on the fact that CHT has not yet been approved by Food and Drug Administration (FDA) for the use in pulmonary delivery. In order to be cleared out by the kidneys, CHT should be degraded by enzymes capable to hydrolyze glucosamine-glucosamine, glucosamine-N-acetyl-glucosamine and N-acetyl-glucosamine-N-acetyl-glucosamine linkages, such as lysozyme, which is also present in the lung mucosa. Moreover, when tested in laboratory mice its LD_{50} was found to be similar to sugars and salt. When placed with living samples, CHT-based biomaterials show that there are little to no inflammatory or allergic reactions.[76,80]

When in contact with lungs, the interaction between CHT and lung mucosa is characterized by molecular attractive forces due to electrostatic interactions between positively charged CHT and negatively charged mucosal surfaces, promoting drug transmucosal absorption.[81,82] Since CHT has a gelling ability when in contact with aqueous solution microparticles can be used as carriers, the drug is released due to the gelling ability of CHT because when it contacts with aqueous solutions, the polymeric chain begins to swell as water enters the small holes between each chain. Also, it has recently been confirmed that CHT has a drug adsorption-enhancing effect in pulmonary tissues by opening of the intercellular junction of the lung epithelium, as well as improving drug targeting and dissolution rate of drugs.[76,81,83] Since CHT is soluble in weak acidic solutions, the production of microparticles

offers the possibility of avoiding hazardous organic solvents. Also, CHT has a good ability to control the release of active pharmaceutical ingredients (APIs), making it a material of interest to produce and develop drug release systems. Therefore, CHT is here used for pulmonary drug administration, as a biodegradable, biocompatible and non-toxic excipient by producing dry powder formulations. The use of dry powders as drug delivery systems has been increasingly considered as a treatment option, even though it brings out concerns related to respiratory tract anatomy, breathing pattern and particle size. Ideally, dry powders should have high dispersibility, drug stability, narrow size distribution and sustained release. Above all, there is a need to control both size and morphology of the particles since those are the characteristics that affect drug deposition. There is also a need to assure that the particles have a physical stability in order to prevent unfavorable solid-state transitions.[81]

1.9 Characterization of particles

Both the European and US pharmacopeia recommend the use of Andersen Cascade Impactor (ACI) and Next Generation Impactor (NGI) when testing inhaling products. [84] ACI is a sizing sampler containing 8 aluminum stages, each with a collection plate and a filter, and an induction port with a suitable mouth piece adapter, operating on the principle of inertial impaction. The impaction of a particle is dependent on its aerodynamic diameter, for example, if particles have sufficient inertia they will deposit on the first stages of the ACI; if particles have smaller sizes, they will remain entrained in the air stream and will pass onto the next stage. This process is repeated until the last stage of the ACI. Therefore, smaller particles are collected in the last stages. ACI is presented vertically and each collection plate corresponds to a determined cut-off diameter, as seen in Figure 1.9.[84]

Collection Plate	Cut-off diameter (µm)
6	0.26
5	0.55
4	1.2
3	1.9
2	3.2
1	4.4
0	6.5
-1	8.6

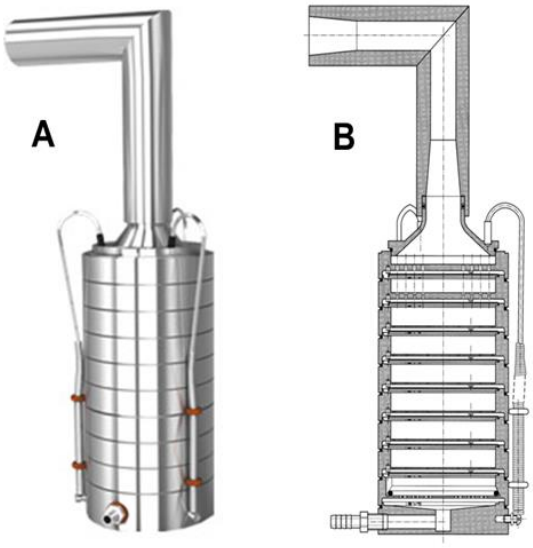

Figure 1.9 Collection plates and their corresponding cut-off diameter (µm)for an Anderson Cascade Impactor with an air flow rate of 60 L/min at a pressure drop of 4 kPa .A – schematic representation of an ACI and B – schematic representation seen from inside

All stages have a decrease in the nozzles' diameter throughout the apparatus. The airflow rate should provide a pressure drop of 4 kPa with a defined time that allows the passage of 4 liters of air through the ACI. [84,85] A schematic representation can be seen in Figure 1.9.

Particle size is estimated considering the amount of particles collected in each stage of the ACI (mass distribution), and can be determined by UV spectroscopy of HPLC.[86] Fine particle fraction (FPF) can also be estimated as being the amount of particles with a cut-off diameter bellow 5 µm. An important parameter to take into account is the aerodynamic diameter, which is diameter of spheres with unit density, able to reach the same velocity in the air stream as particles of arbitrary shape and density. From this analysis we can also obtain another important parameter, the mass median aerodynamic diameter (MMAD), which corresponds to the particles' aerodynamic diameter at 50% of the particle size distribution. It is known that particles having a MMAD between 1-5 µm, are easily deposited in the bronchial and alveolar regions, especially by sedimentation. These particles have the best pulmonary penetration being in the ideal size range for the majority oral inhalation products.[87]

Another important characteristic of the pharmaceuticals is its solid-state chemistry. For lung delivery, the carrier should be amorphous since it shows high dissolution rates, high water adsorption and also it is crucial for storage purposes while the API must be crystalline so that the bioavailability is maintained.[21] Nonetheless, and contrarily to crystalline forms,

amorphous compounds are defined by a disorder arrangement of its molecules, showing less stability and more reactivity.[21,88]

Besides the amorphous structure and sizes between 1-5 µm, particles should have smooth surfaces and a small contact area, reducing drug adhesion and therefore promoting a better drug release and increasing the distance between particles, which will reduce interparticulate forces. All this combined will then lead to a better particle performance.[21,89] In order to address particles' surface area, a Brunauer – Emmett – Teller (BET) analyses is performed. This analysis is based on BET equation is only valid to solid surfaces. Adsorption occurs when a fluid gets in contact with a solid surface by interactions between them, involving two main forces: physical forces (based on small Van der Waals forces) or chemical adsorption (based on chemical bonding between molecules). Although there are six types of isotherms, according to IUPAC, herein we describe the Type II sorption isotherm, which can be explained by BET equation. [89,90] This type is commonly obtained in the case of non or macroporous adsorbent, where unrestricted monolayer-multilayer adsorption can occur. An inflection point on the isotherm indicates the phase at which the monolayer adsorption is complete, and multilayer adsorption begins. In addition to these characteristics, particles presenting low relative humidity (< 50%) show insignificant capillary forces, however particles with higher relative humidity present strong capillary forces and therefore higher adhesion forces between the drug and the carrier.[21]

In order to provide a sustained controlled release, drug-polymer systems were produced and because of that the release of the drug is dependent not only in the diffusion rate from the non-degraded polymer, but also by its swelling and erosion.[91,92] There are two different phases during particles swelling: a glassy polymer phase and a rubbery-solvent phase. When there is no water penetrating the system, the relaxation does not occur and the drug is released by Fickian diffusion through the glassy polymer. However, if water can indeed enter the polymeric matrix, a "Case-II transport" occurs, which means that we are in the presence of a sharp advancing interface at constant velocity, resulting in a zero-order drug release. Most of the times, these two mechanisms occur at the same time, providing an "anomalous transport". This is due to the fact that both relaxation and diffusion transport occur.[91,92]

When it comes to model the drug release out of polymeric matrices, the Korsmeyer-Peppas equation (equation 1) has been the most used one to study the diffusional exponent, *n*, which indicates the transport mechanism. The mechanism can either be due to the Fickian diffusional release (n=0.43) or polymer's swelling (n=0.85). It also considers a *k* that is a

of the macromolecular network system of the drug. However, it is only valid to the first 60% of the release, because the further release is dependent on other factors that are not taken into account, such as particles degradation.[93]

$$\frac{M_t}{M_\infty} = k.t^n \quad (1)$$

1.10 Work thematic

In the present work, a system combining strawberry-like gold coated magnetite nanoparticles encapsulated into CHT were developed. Dry powders of the nano-in-micro formulations were produced using SASD apparatus. The powders were characterized in terms of morphology, physical-chemical and solid state properties and in terms of aerodynamic performance. Also, in order to assess the releasing profile of nanoparticles from the CHT microparticles, a release study was performed.

Since these formulations are supposed to be used as pulmonary drug delivery systems to fight lung cancer, a model drug was encapsulated and the release profile of the drug from the microparticles was also assessed.

Figure 1.10 shows a schematic representation of the mechanism of action of this system. First, the powders should have desired properties for inhalation. Once inhaled, the microparticles containing the nanoparticles and the drug are supposed to deposit in the deep lung region (lung epithelia) and CHT degrades releasing the nanoparticles and the drug. Since the nanoparticles are protected with oxazoline, they are protected from degradation. The same thing happens to the drug. Once released from the CHT microspheres, nanoparticles undergo an endocytosis process and enter the cancerous cell. Here, they release the drug, leading to the death of the lung cancer cell.

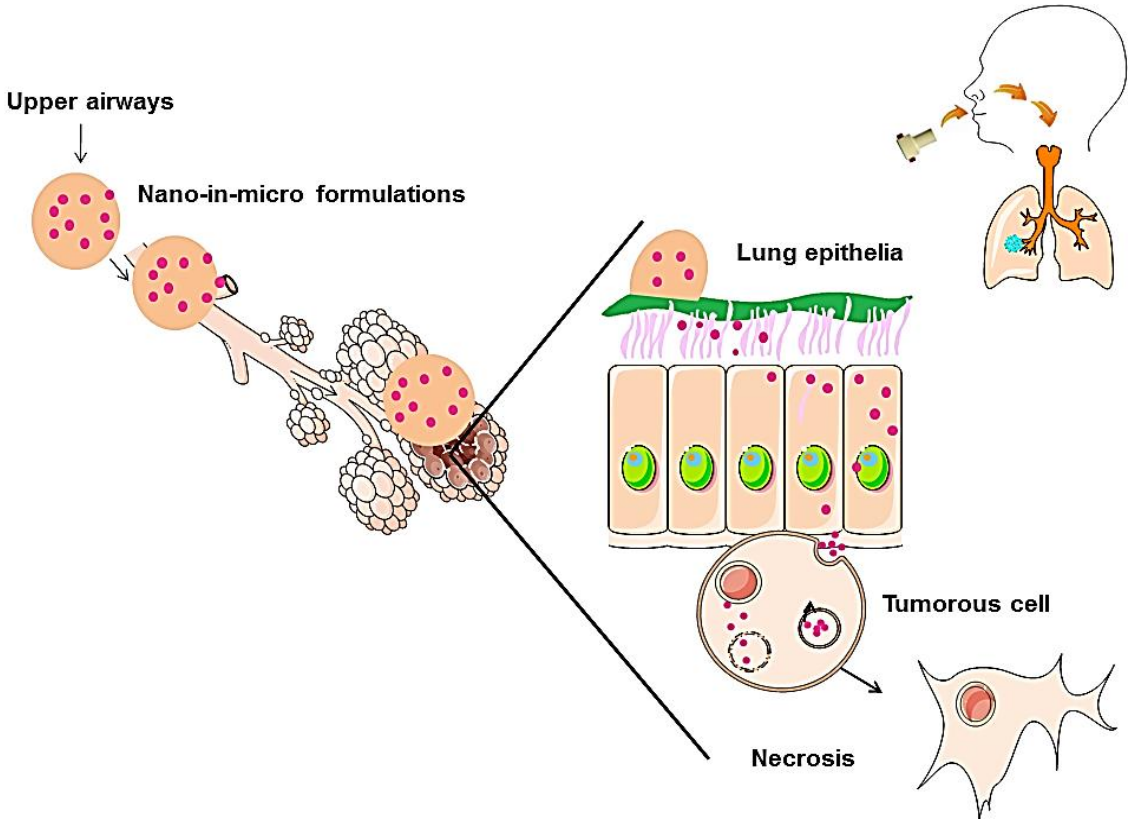

Figure 1.10 Schematic representation of the mechanism of action of this system

2

Experimental Section

2.1 Materials

All components were used as received without any further purification. Chitosan (viscosity 5-20 mPa.s) was purchased from Tokyo Chemical Industry. Cysteamine (99%) was purchased from Sigma Aldrich. Ethanol (EtOH) (96% purity) was purchased in Panreac. Industrial carbon dioxide (CO_2, purity ≥ 99.93%) was obtained from Air Liquide. The monomer 2-ethyl-2-oxazoline (EtOx, ≥ 99% purity), boron trifluoride diethyl etherate ($BF_3.OEt_2$), diethyl ether, acetic acid glacial (99.7% purity) hydrogen tetrachloroaurate 99%, sodium citrate 99%, sodium hydroxide, potassium nitrate, sulphuric acid, ferric sulphate, poly-diallyldimethylammonium chloride (PDADMAC), poly-sodium styrenesulfonate (PSS) and methanol (MeOH) were purchased from Sigma Aldrich.

2.2 Methods

2.2.1 Synthesis of the strawberry-like gold coated magnetite nanoparticles

This synthesis was performed following a recent published methodology in the BIO-SCOPE Lab 308. This methodology included three synthetic steps.[62]

2.2.1.1 Fe_2O_3 nanoparticles - $Fe@SO_4^{2-}$

$Fe@SO_4^{2-}$ was synthesized by modifying a method described by M. A. Vergés *et al*. [94] In this step occurs the precipitation and aging of magnetite nanoparticles. Two different solutions were prepared. A solution (A) containing 90 mL of distilled water, and 90 mL of absolute ethanol with NaOH $7x10^{-2}$ M (12.6 mmol; 0.504g) and KNO_3 0.1 M (18 mmol; 1.8384g) was placed in a three-necked round bottom flask. A second solution (B) was prepared using 10 mL

of distilled water and 10 mL of absolute ethanol containing H_2SO_4 $1x10^{-2}$ M and $Fe(SO_4)_2$ $5x10^{-2}$ M (1 mmol; 0.2808 g). Both solutions were kept under inert atmosphere separately for one hour. Maintaining the nitrogen atmosphere, solution (B) was drop-wise to solution (A). When precipitation ended, the nitrogen bubbling was continued for ten minutes. All the reaction mixture was heated at 90 °C for 24 h.

In the end of the reaction, the round bottom flask was cooled in an ice/water bath. The solid magnetic nanoparticles were separated by magnetic decantation and washed five times with distilled water. The final magnetic solid was re-suspended in 80 mL of Milli-Q water. Strong magnetite nanoparticles with near cube-shaped were obtained.

2.2.1.2 Gold nanoparticles (AuNP)

First, Au@citrate nanoparticles were prepared in aqueous solution following the-Turkevich methodology.[95] An aqueous solution (125 mL) of hydrogen tetrachloroaurate (0.125 mmol, 49.5 mg) was added rapidly to a solution of 1% (w/v) (0.125 g) sodium citrate (12.5 mL). Both the solutions were heated and the addition only occurs when both of them are near the boiling point. After mixing them, the heating was maintained for an additional 5 min. During this time, the color changed to deep red.

2.2.1.3 Strawberry-like gold coated magnetite nanoparticles: gold-shell formation

In the third step, following a previous procedure described by Caruso et al.[96–98] poly-diallyldimethylammonium chloride (PDADMAC) and poly-sodium 4-styrenesulfonate (PSS) were alternately adsorbed onto the negative surface of the magnetic nanoparticles $Fe@SO_4^{2-}$. A solution of 5 mL of the previous $Fe@SO_4^{2-}$synthesized NPs was re-suspended in 100 mL of milli-Q water during 2 minutes assisted with ultrasonic energy. 100 mL of a water solution containing 1mg/mL of PDADMAC was added. The solution was maintained in an ultrasonic bath during a minute, and under magnetic stirring during two 2 hours. The NPs obtained were separated from the supernatant by magnetic separation and washed 10 times with milli-Q water. This process was repeated for the adsorption of the PSS layer, and for a second monolayer of PDADMAC.

The three-layer polyelectrolyte magnetite nanoparticles washed previously, were re-suspended in 100 mL of milli-Q water and mixed with 5 mL of NaCl 0.2 M solution. This solution was kept during one minute in an ultrasonic bath. After this time, 20 mL of previously synthesized gold nanoparticles was added, and the entire solution was maintained with magnetic stirring during 2 hours. The final nanoparticles were separated from the supernatant by mag-

netic decantation, and washed ten times with milli-Q water being finally re-suspended in 100 mL of Milli-Q water.

The formation and growth of the partial gold shell was performed by adding to the solution an aliquot of 100 µL of Au^{3+} ($5x10^{-4}$ M) followed by the addition of 100 µL of ascorbic acid ($0.34x10^{3}$ M) under ultrasonic stimulation to help nanoparticle separation during the growth process. The strawberry-like nanostructures Fe@Au NPs were separated by magnetic decantation and washed ten times with milli-Q water. Subsequently they were re-suspended in 20 mL of milli-Q water.

Samples for TEM were prepared by pipetting a drop of the colloidal dispersion onto an ultrathin carbon coated copper grid and allowing the solvent to evaporate.

2.2.1.4 Nanocomposite functionalization with Oligo(2-ethyl-2-oxazoline)s terminated with cysteamine

The Fe@Au NPs were suspended in 10 mL of milliQ water and were placed in a flask reaction. Under stirring in a US bath was added drop-wise 5 mL of polymer solution in MeOH (5 mg/mL). NPs were kept under magnetic stirring overnight. Afterwards, the nanoparticles were washed in MeOH twice. The final material obtained shows high solubility in MeOH. During repeated magnetic cycles of purification, we have observed for the first supernatant a subtle red colour, mainly derived a small percentage of gold nuclei released during functionalization. However, as proved by TEM microscopy, the final nanomaterial obtained possesses the strawberry structure with the AuNPs anchored to the surface of the magnetic cores.

2.2.2 Synthesis of the living oligo(2-oxazoline)

The polymerization was carried out following the procedure described by C. Macedo *et al.*[74] Thus, 2-ethyl-2-oxazoline monomer and the initiator $BF_3.OEt_2$ were both added to a high-pressure stainless-steel reactor, being the monomer/initiator ratio of [M]/[I] = 1/12 . The reaction was carried under stirring conditions and the reactor cell was placed in a water bath at 60°C. Carbon dioxide was introduced in the reactor until it reached 160 bar. After 24 hours of reaction, a continuous washing process was taken using $scCO_2$ for 1 hour. After the washing process was concluded, the pressure was slowly released until the reactor reached room temperature. A viscous foam was obtained inside the reactor.[69]

2.2.2.1 End-capping of living oligo(2-ethyl-2-oxazoline)s with cysteamine

The living oligo(2-ethyl-2-oxazoline) was end-capped with cysteamine, this process is performed by adding a tenfold excess of cysteamine (OligoSH) solubilized in anhydrous DMF, relatively to the initiator. The mixtures were kept at 70 °C using an oil bath under stirring for 24 hours. To the oily oligomer solubilized in dry DMF was added diethyl ether and an extraction step was performed in order to remove any unreacted oxazoline. This step was repeated four times until the diethyl ether phase showed no evidence of impurities. Then, to the aqueous phase, a known amount of water was added and the polymer was purified by dialyses against pure milliQ water. The resulting mixture was dried under vacuum and the resulting oily polymer presented a yellow brownish color with a yield of 6%.[69]

2.2.3 Particle production – SASD apparatus

SASD apparatus consists on the mixture of $scCO_2$ with a casting solution containing CHT and the nanoparticles. Therefore, solutions of 1% (w/v), 2% (w/v) CHT (dissolved in 1% acidic water) with and without Ibuprofen and NPs were prepared. All the solutions were atomized and in order to accomplish that, CO_2 is liquefied in a cryogenic bath (-20ºC) and pumped with a high-pressure liquid pump (HPLC pump K-501, Knauer), which was then heated in an oil bath (70°C) and sent to the static mixer (model 37-03-075, Kenics-Chemineer, 4.8 mm ID x 191 mm L, 27 helical mixing elements). A high-pressure pump (HPLC 305, Gilson) was used to pressurize the casting solution into the static mixer, which allows the solubilization of the CO_2 into the liquid solution due to its high surface packing, promoting the near equilibrium. In order to maintain CO_2 in its supercritical state (above 73.8 bar and 31 °C),[27] the static mixer is enrolled by heating tapes controlled by a shinko FCS-13A temperature controller (0.2 °C resolution). The pressure in the static mixure is measured using a Setra pressure transducer (0.1 psig stability). The mixture was then sprayed through a 150 µm diameter pressure nozzle into an aluminum precipitator (± 0.1 °C), where the primary droplets are formed, and which operates at near-atmospheric conditions. At the same time, a continuous compressed heated air flow enters into the precipitator and dries the particles by evaporating the liquid solvent and promoting the expansion of CO_2 from the inside of these primary droplets, originating the secondary droplets. The compressed air flow is heated before entering the precipitator. The formed and dried particles exit the precipitator from the bottom side and enter into a high-efficiency (Bucchi) cyclone where they are separated from the gas stream and collected in a glass flask, placed under the high efficiency cyclone [32]

2.3 Particles Characterization

2.3.1 Characterization of nanoparticles

2.3.1.1 Dynamic light cattering, Zeta Potential and TEM analyses

The size measurements were performed with the end-capped nanoparticles diluted in 3mL of methanol in a Zetasizer Nano ZS instrument (Malvern Instruments) in the PROTEO-MASS facilities. Zeta potential quantification was carried out in the same Zetasizer Nano ZS instrument using a zeta dip cell. TEM analysis was performed in Spain, in the University of Vigo, CACTI (Center for Researcher and Technical Assistance).

2.3.1.2 UV-Vis spectra and fluorescent analyses

The UV-Vis spectra of the nanoparticles herein developed were acquired using Perkin Elmer Lambda 25 UV/Vis Spectrometer with a slit width of 5 nm at a scan rate of 240 nm min^{-1} at 25 ºC, in a wavelength range from 350 to 750 nm, and then analyzed with PerkinElmer UV WinLab™ software. Fluorescence assays were also performed on a PerkinElmer LS 45 Luminescence Spectrometer with a slit width of 5 nm at a scan rate of 240 nm min^{-1} using a 10 mm path quartz cell and analyzed using FL WinLab™ software. The excitation wavelength was fixed at 300 nm.[69]

2.3.1.3 FT-IR Spectra and ^{1}H NMR

The ^{1}H NMR spectra of the oligo(2-oxazoline) terminated with cysteamine (OEtOxSH) was acquired in a Bruker ARX 400 spectrometer. CHT, Fe@Au_OEtOxSH and CHT_Fe@Au_OEtOxSH were also analyzed in a Fourier transform infrared (FT-IR) with a resolution of 1 cm^{-1} and 16 scans per sample on a Tensor 27 FTIR (Bruker) coupled with Opus Spectroscopy Software.

2.3.2 Characterization of microparticles

2.3.2.1 Morphologi G3 and SEM analyzes

Particle size analysis was performed by a particle analyzer system (Morphologi G3 Essentials, from Malvern Instruments Ltd). The particles were characterized by the volume mean diameter (Dv) and the relative width of the distribution, span, calculated as follows:

$$\text{Span} = \frac{D_{v,90} - D_{v,10}}{D_{v,50}} \qquad (2)$$

where $Dv_{,90}$, $Dv_{,10}$ and $Dv_{,50}$ are the diameters at 90%, 10% and 50% cumulative volume. Microparticles morphology was determined via Scanning Electron Microscopy (SEM) (Hitachi, S-2400 instrument) with an accelerating voltage set to 15 kV and magnifications of 500 and 10k. All the samples were mounted on aluminum stubs using carbon tape and were gold-coated pri-ori analysis. Tapped density of microparticles was determined by compressing a known mass of powder in a volumetric container, and measuring the final volume. [46]

2.3.2.2 FT-IR Spectra, XRD and BET Analyses

FT-IR was performed in order to study the interactions between CHT and the NP. The FT-IR spectra of the materials was done using potassium bromide (KBr) tablets (1% w/w of powder in KBr) with a resolution of 1 cm^{-1} and 16 scans per sample on a Tensor 27 FT-IR (Bruker) coupled with Opus Spectroscopy Software.

In order to determine whether the particles were crystalline or amorphous, samples of powders were subjected to X-ray diffraction (XRD) analysis (RIGAKU X-ray diffractometer, model Miniflex II). Samples were placed in a holder and analyzed through CuKα radiation (30 KV/15 mA), with a 2θ angle ranging between 2° and 55° with a scan rate of 1°/min.

BET specific surface area was determined in a Micromeritics ASAP 2010 Physisorption Analyser, using 50 mg samples. The analysis was performed in two phases, first by heating the sample up to 320 K for 42 h, in order to release all adsorbed gases in the particle. Secondly, the temperature was lowered and maintained at 77.35 K during the time of the analysis.

2.3.2.3 Karl Fischer coulometric titration

Water content of each sample was accessed using Karl Fischer coulometric titration. 1.5 mg of each sample was placed into the titration vessel and titrated with Karl Fischer reagent, which reacts quantitatively and selectively with water. The instrument was composed by the 831 KF Coulometer and a 728 stirrer Metrohm and by a Pt /-20 -70 °C electrode.

2.3.2.4 Aerodynamic performance of the produced nano-in-micro formulations [32,99]

Andersen Cascade Impactor (ACI) equipment was used to measure the median aerodynamic particle size, which is seen as a function of density and viscosity as well as the physical

dimensions and shape of the particles under development. Such parameter is important since it helps to explain how particles behave in a moving air stream (as exemplified by the respiratory tract) as opposed to simple “geometric” size. The eight stages of the Andersen Cascade Impactor (ACI) were used to determine the emitted fraction (EF) and respirable fraction (RF) of the microparticle powders. The capsule was punctured prior to inhalation and a pump was actuated to simulate an inspiration (air flow rate of 62.9 L/min during 3.9 s). Three capsules were emptied sequentially for each run. The EF corresponding to the percentage of total loaded powder mass exiting the capsules was determined gravimetrically and can be expressed as the emitted fraction (EF%) corresponding to the total loaded powder exiting the capsule, and was calculated as follows:

$$EF(\%) = \frac{m_{full} - m_{empty}}{m_{powder}} \text{ x } 100 \quad (3)$$

where full and empty are the weights (mg) of the capsule before and after simulating the inhalation and powder is the initial weight (mg) of the powder in the capsule.

The amount of particles entering our respiratory tract (respirable fraction) was calculated by subtracting the amount of the particles trapped inside the capsules to the amount of particles trapped inside the induction port.

Fine particle fraction (FPF) was determined by the interpolation of the amount of particles (in percentage) with a diameter bellow 5 µm emitted from the capsules in each experiment. Mass median aerodynamic diameter (MMAD) was calculated as the particle diameter corresponding to 50% the cumulative distribution. Geometric standard deviation (GSD) was determined considering the d_{84} and d_{16} measures, which are the diameters corresponding to 84% and 16% of the cumulative distribution, respectively, and can be calculated by the following equation:

$$GSD = \sqrt{\frac{d_{84}}{d_{16}}} \quad (4)$$

2.3.2.5 Entrapment Efficiency

The drug encapsulation was determined by milling a fixed amount of co-atomized powders and then adding a known amount of PBS. The solution was agitated for 2 h and then was centrifuged at 15 000 rpm for 5 min. The supernatant was then collected and the amount of drug was determined by UV spectroscopy at 225 nm for IBP. In order to know the entrapment

efficiency of the nanoparticles into the CHT microparticles, a sample of 20mg of powder was resuspended in aqua regia and the amount of gold and iron was measured through ICP analysis. The encapsulation (E%) was determined by:

$$E\% = \frac{m_r}{m_i} x\ 100 \quad (5)$$

where m_r is the remained mass and m_i is the initially uploaded mass.

2.3.2.6 *In vitro* Cumulative Release studies [92,100]

To evaluate the percentage of nanoparticles and IBP that were released from the microparticles, 20 mg of the CHT_Fe@Au_OEtOxSH and CHT_Fe@Au_OEtOxSH_IBP powders were transferred into a snake skin membrane with a cut size of 1µm and incubated into 5mL of different pHs solutions in a shaking bath (36 rpm and 37ºC): 7.4 and 6.8, pH of an healthy cell and pH of a cancer cell, respectively. At different time intervals, 1mL of each solution was taken and another mL of fresh solution was placed. The absorbance from each sample was read using a UV-Vis spectrophotometer (225 nm in the case of IBP). This way it is possible to know the amount of IBP released from the microparticles. The release profile was adjusted to Korsmeyer-Peppas mathematical model and the n-value was obtained from the slope of the Korsmeyer-Peppas plot and represents different release mechanisms. For spherical geometries: n = 0.43 for Fickian diffusion; 0.43 < n < 0.85 for anomalous non-Fickian diffusion; n = 0.85 for Case-II transport. In both cases herein described we have obtained a non-Fickian diffusion, since n = 0.59 for pH 7.4 and n = 0.61 for pH 6.4.

Another study was carried: two samples of CHT_Fe@Au_OEtOxSH powder were transferred to a snake skin membrane and were placed in 5mL of pH 7.4 and pH 6.8. Both the solutions were placed on top of a magnet and after 5 hours and 24 hours a photo was taken. This study enables to understand if, upon nanoparticles release from the micropowders, their magnetism is maintained.

3

Results and Discussion

3.1 Nanoparticles Characterization

All nanoparticles have been characterized in terms of their size and zeta potential. These characterizations are important since nanoparticles should not exhibit sizes larger than 150 nm.[42] Notwithstanding, particles comprising sizes ranging between 20 to 50 nm have shown to have higher cellular internalization.[43,101] It has also been proved that nanoparticles with non-cationic surface charge are used in pulmonary delivery since they can be rapidly translocated from the lung epithelium to mediastinal lymph nodes. This should provide high levels of drug to pulmonary lymph nodes, which could be used to deliver antibiotics and anti-inflammatory drugs to treat other lung infections, tumor metastases and inflammatory conditions.[44] Therefore it is important to study the size and potential of the produced nanoparticles. Size measurements are not viable in this type of nanoparticles once they tend to agglomerate in solution, therefore conferring low viability during the measurements. Zeta Potential was measured in each step of the procedure. The first measurement was performed to the initial nanoparticles without any polymeric layer showing a negative potential. Then, after the first addition of the first polymeric layer (positively charged polymer) the zeta potential turned positive, proving that the first layer was coating the Fe nanoparticles. The same was done for the second layer (negatively charged polymer) and for the third (positively charged polymer) and zeta turned negative and then positive again. The final nanoparticles composed of the magnetite nanoparticles, the three polymeric layers, the gold shell and the coating with the oxazoline showed a positive potential, of around 33.6 mV (Figure 3.11). Having a positive potential at the surface, nanoparticles are supposed to be easily internalized since the phospholipidic membrane is negatively charged. Colloidal dispersion stability is well dependent they depend on their zeta potential. For values ranging between +- 30 to +- 40 mV there is a moderate stability, on the other hand values ranging from +- 10 to +- 30 mV may result in some particle's instability which may result in some particle aggregation Their sizes are well-suited for delivery into tumoral microenvironments As seen, TEM

images (Figure 3.12) were analyzed with JImage® and the average size of the nanoparticles is around 100 nm. As a proof-of-concept, this system proves to have the ideal conditions for cell internalization.

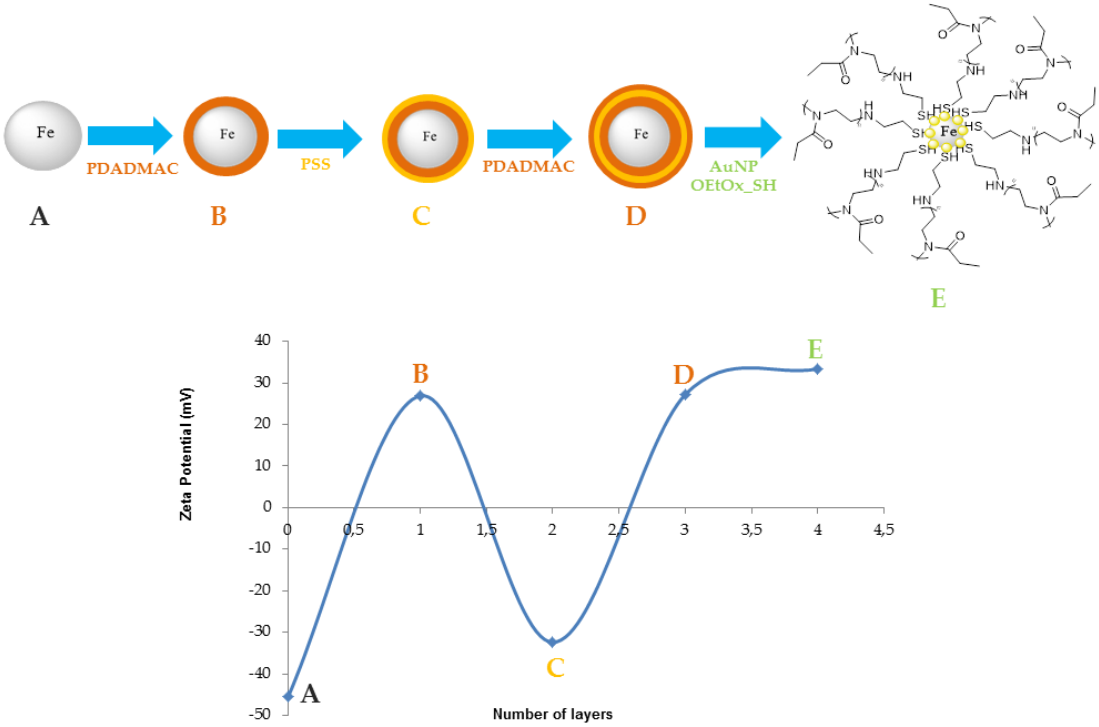

Figure 3.11 Zeta potential of the different layers, where the 4th layer corresponds to the final nanoparticles

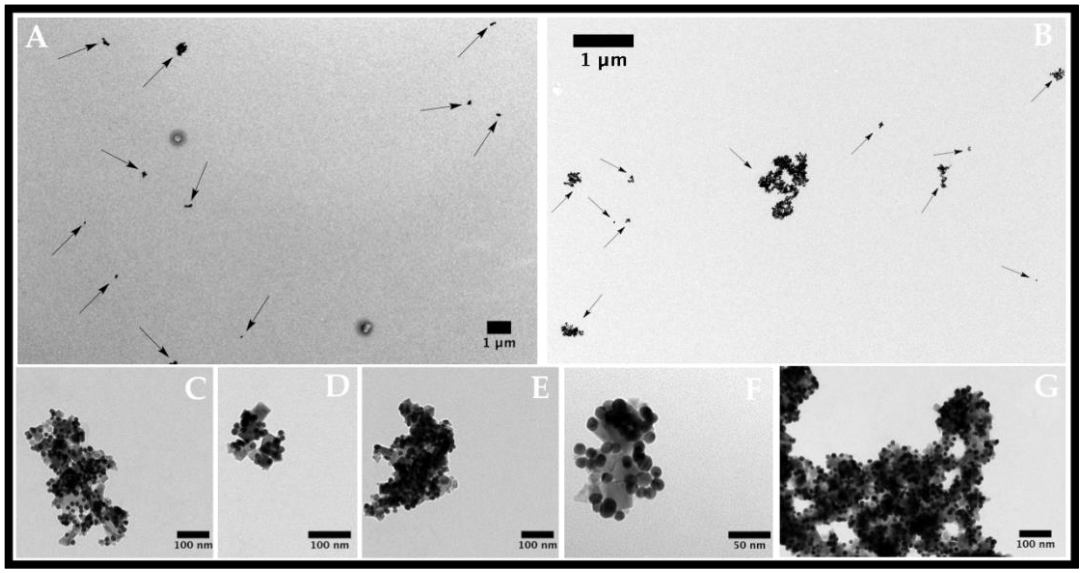

Figure 3.12 Transmission Electron Microscopy images of strawberry Fe/Au nanomaterial functionalized with oligo(2-ethyl-2-oxazoline)s in different magnifications. A and B – magnetite nanoparticles; C, D, E, F and G – Strawberry-like gold magnetite nanoparticles functionalized with oligo(2-oxazoline)

UV-Vis and fluorescent assays were performed in order to corroborate that the oligo(2-ethyl-2-oxazoline) terminated with cysteamine was, in fact, bonded to the surface of the nanoparticle. Since magnetite gold-coated nanoparticles do not present any fluorescence, then, as we add a fluorescent polymer it is expected to observe the presence of an emission band. This band can be observed in Figure 3.13, where the emission and the absorption of the final nanoparticles are compared.

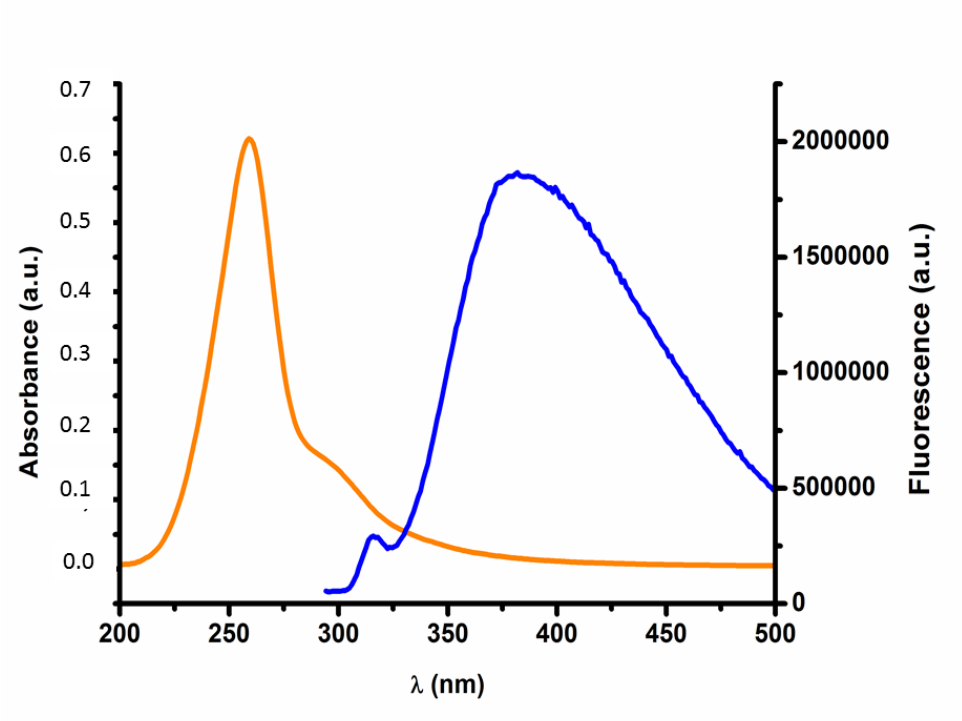

Figure 3.13 Fluorescence vs Absorbance of the final nanoparticles. The emission band can be denoted at 384 nm (orange line) and the absorption band can be seen at 300 nm (blue line).

3.2 Design of Experience: CHT and CHT_Ibuprofen

In order to evaluate which were the best conditions to operate when producing the microparticles, and since a preliminary study proved that microparticles did not change their characteristics by adding nanoparticles, a DoE was performed for the CHT formulations and CHT_IBP formulations. In each assay three conditions were changed: pressure in the static mixer (1300 - 1600 psi); CHT concentration (1% - 2% (w/v)); and solution flow rate (2 – 5 mL/min). In order to perform these experiments, a cube was designed and each vertex corresponds to an assay and can be observed in Figure 3.12.

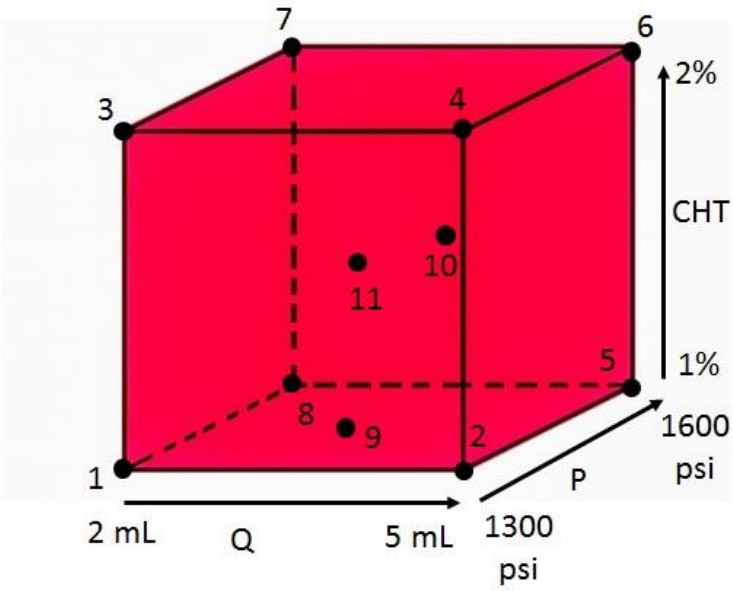

Figure 3.14 Design of Experiment for CHT and CHT_IBP assays

All the powders obtained in each assay were characterized via ACI analysis and the best formulation was chosen concerning the FPF, EF, MMAD, Dv_{50} and yield. The following Tables present the conditions of each assay (Table 1) and the characterizations performed (Table 2 and Table 3).

Table 1 Operating conditions for DoE CHT assays

Assay	$P_{\text{static mixer}}$ (psi)	Solid Concentration (% w/v)	$Q_{solution}$ (ml/min)	Q_{CO_2} (ml/min)	Q_{air} (kg/h)	T_{air} (in) (°C)	T_{air} (out) (°C)	T_{CO_2} (°C)	$T_{cryostate}$ (°C)	$T_{\text{static mixer}}$ (°C)
1	1300	1	2	25	22	109.5	76.5	90	-20	80
2	1300	1	5	25	22	109.5	70	90	-20	80
3	1300	2	2	25	22	109.5	70.4	104	-20	80
4	1300	2	5	25	22	109.5	68.9	85	-20	80
5	1600	1	5	25	22	109.5	67.8	91	-20	80
6	1600	2	5	25	22	109.5	70.9	79	-20	80
7	1600	2	2	25	22	109.5	71.4	80	-20	80
8	1600	1	2	25	22	109.5	75.2	90	-20	80
9	1300	1.5	3.5	25	22	109.5	67.9	92	-20	80
10	1600	1.5	3.5	25	22	109.5	71.4	91	-20	80
11	1450	1.5	3.5	25	22	109.5	69.9	94	-20	80
12	1450	1.5	3.5	25	22	109.5	67.1	96	-20	80

Q – flow; **T** - temperature; **P** – pressure

Table 2 Aerodynamic properties of CHT dry powders and yield

Assay	MMAD (μm)	RF (%)	FPF (%)	GSD (%)	EF (%)	Yield, η (%)
1	0.9	65	42.1	2.4	95.8	51
2	1.1	71	55.8	2.7	98.5	68
3	1.0	66	53	2.4	95.7	63
4	1.4	72.6	53.5	2.6	99	55
5	1.4	68.5	54.6	2.4	98	88
6	1.5	78.5	59.1	2.6	99	78
7	1.1	59.2	45.4	2.7	98.5	66
8	1.1	55.1	37.9	3.1	98	70
9	1.3	64.8	51.8	2.8	98	71
10	1.4	48.6	34.7	2.9	99	74
11	1.3	59.1	46.2	2.9	98.5	72
12	1.2	58.2	44.3	2.7	99	73

MMAD – Mass Median Aerodynamic Diameter; **RF** – Respirable Fraction; **FPF**- Fine Particle Fraction; **GSD** – Geometric Standard Deviation; **EF** – Emitted Fraction

Table 3 Morphologi G3 results for the produced CHT powders

Assay	$D_{v,10}$	$D_{v,50}$	$D_{v,90}$	Span
1	1.9	3.3	6.3	1.3
2	1.9	3.1	4.6	0.9
3	2.5	4.3	6.6	0.9
4	3.6	5.6	9.0	1.0
5	3.2	4.5	9.1	1.1
6	2.7	5.8	9.1	1.1
7	1.5	2.9	4.5	1.1
8	0.8	1.6	3.6	1.8
9	2.7	5.7	9.6	1.2
10	2.9	6.7	10.4	1.1
11	3.2	7.3	11.6	1.2
12	2.4	5.0	8.7	1.3

Dv50 – mean volume diameter; **Dv90** and **Dv10** – volume diameters at 90 and 10% of the population

The deposition of the particles during the different stages of ACI, mimetizing the different stages of the lung, can be observed in Figure 3.13.

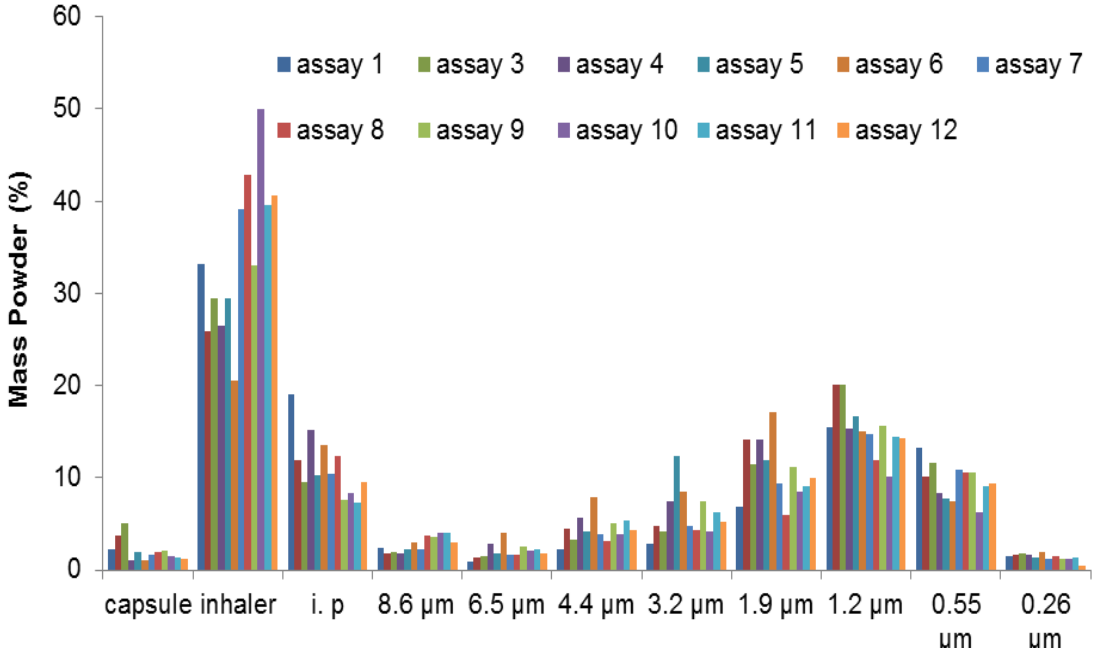

Figure 3.15 Representation of the distribution of CHT powders through the different stages of the ACI

As seen in the Tables and in Figure 3.15 (ACI), the best assays obtained, bearing in mind the FPF, EF, MMAD, D_{v50} and yield were assay 5 and 6. However, once the differences between them are not significant, the assay chosen to continue with the encapsulation process of the nanoparticles into the CHT microparticles was assay 5, once it needs lower doses of CHT. By doing this experiment, it was possible to understand that the most influencing parameters in this process are both the pressure of the static mixer and the flow rate of the solution. As seen, higher pressures and higher flows, originate better powders, with better aerodynamic properties. In terms of shape, all the particles were similar, once all the particles had a spherical shape, as seen in Figure 3.16.

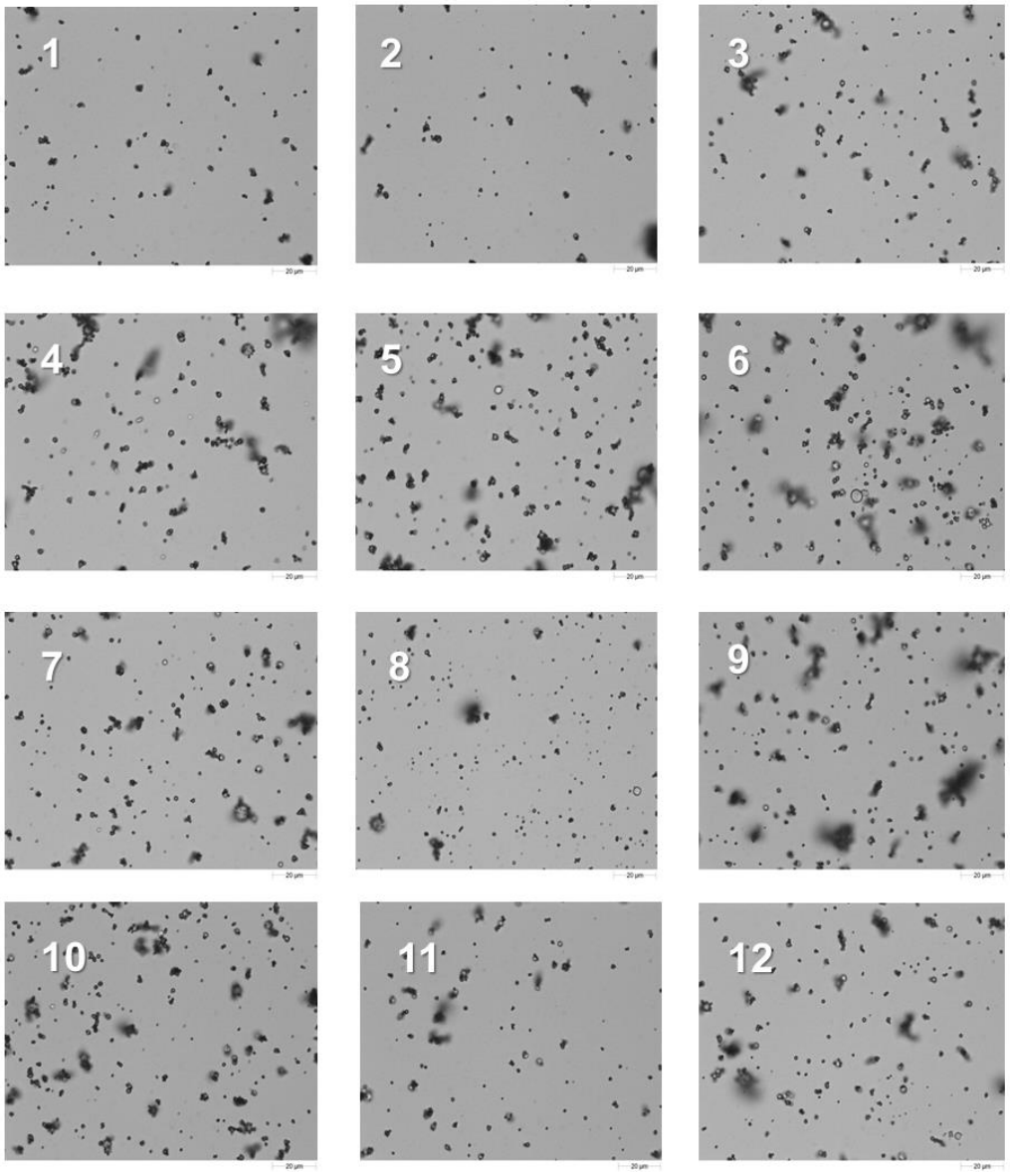

Figure 3.16 Morphologi G3 images of the produced CHT powders

The same studies were performed in order to evaluate which were the best conditions for CHT_IBP formulations. These studies were also based in the same DoE cube. However, in both assays 3 and 7, it was not possible to keep the solution at a flow rate of 2 mL/min. Therefore, an adjustment was executed and for these two assays the solution flow rate was established to 3 mL/min. Also, in assay 3 it was not possible to maintain the pressure of the static mixer around 1300 psi, therefore the assay was performed at 1400 psi.

The conditions are presented in Table 4 and the characterizations made are presented in Tables 5 and 6.

Table 4 Operating conditions for DoE CHT_IBP assays

Assay	**$P_{static\ mixer}$ (psi)**	**Solid Concentration (% w/v)**	**$Q_{solution}$ (ml/min)**	**Q_{CO_2} (ml/min)**	**Q_{air} (kg/h)**	**T_{air} (in) (°C)**	**T_{air} (out) (°C)**	**T_{CO_2} (°C)**	**$T_{cryostate}$ (°C)**	**$T_{static\ mixer}$ (°C)**
1	1300	1	2	25	20	111.5	65.5	92	-20	80
2	1300	1	5	25	20	111.5	72	93	-20	80
3	1400	2	3	25	20	111.5	73.4	95	-20	80
4	1300	2	5	25	20	111.5	68	97	-20	80
5	1600	1	5	25	20	111.5	71.8	93	-20	80
6	1600	2	5	25	20	111.5	70.9	89	-20	80
7	1600	2	5	25	20	111.5	73.6	90	-20	80
8	1600	1	2	25	20	111.5	72.3	90	-20	80
9	1300	1.5	3.5	25	20	111.5	63.9	95	-20	80
10	1600	1.5	3.5	25	20	111.5	73.6	97	-20	80
11	1450	1.5	3.5	25	20	111.5	73.2	96	-20	80
12	1450	1.5	3.5	25	20	111.5	71.6	98	-20	80

Q – flow; **T** - temperature; **P** – pressure

Table 5 Aerodynamic properties of the produced CHT_IBP powders

Assay	MMAD (μm)	RF (%)	FPF (%)	GSD (%)	EF (%)	Yield, η (%)
1	1	79.6	54.5	2.4	98.5	57
2	1.1	82	56.3	2.8	98.6	64
3	1.1	75.9	54.5	2.7	97.2	66
4	1.4	81.7	53.6	2.6	97.5	73
5	1.1	82	56.4	2.6	99	74
6	1.5	78.3	50.6	2.5	96.1	75
7	1.3	72.5	58.4	2.6	94.2	64
8	1.1	73.4	55.2	2.7	95.7	72
9	1.3	73.9	53.3	2.6	95	59
10	1.2	73.8	56.6	2.5	93	70
11	1.1	74.5	57.8	2.6	95.3	62
12	1.1	75	56	2.5	94.9	65

MMAD – Mass Median Aerodynamic Diameter; **RF** – Respirable Fraction; **FPF**- Fine Particle Fraction; **GSD** – Geometric Standard Deviation; **EF** – Emitted Fraction

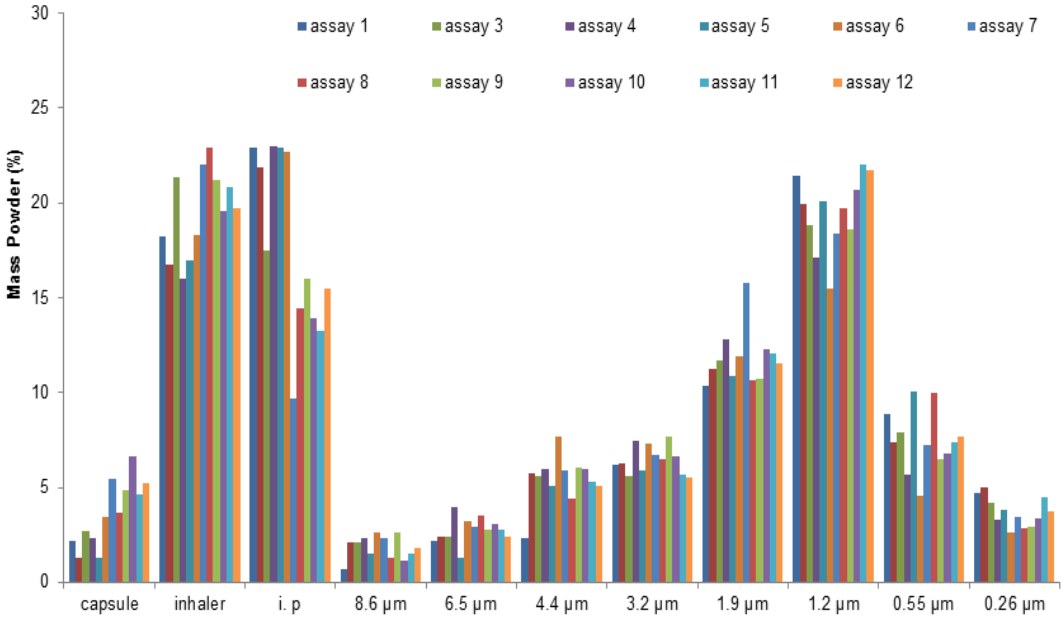

Figure 3.17 Representation of the distribution of CHT_IBP powders through the different stages of the ACI

Table 6 Morphologi G3 results for the produced CHT_IBP powders

Assay	$D_{v,10}$	$D_{v,50}$	$D_{v,90}$	Span
1	2	3.5	5	0.9
2	2	3.6	5.4	0.9
3	3.1	6.7	11.7	1.3
4	2.3	3.8	5.5	0.8
5	2	3.4	5.3	1
6	2.4	4.1	6.1	0.9
7	1.9	3.5	5.2	1
8	1.7	3.1	5.4	1.2
9	1.9	2.9	4.2	0.8
10	2.1	3.5	4.8	0.8
11	1.9	3	4.2	0.8
12	1.7	3.3	4.9	1

D_{v50} – mean volume diameter; **D_{v90}** and **D_{v10}** – volume diameter at 90 and 10% of the population

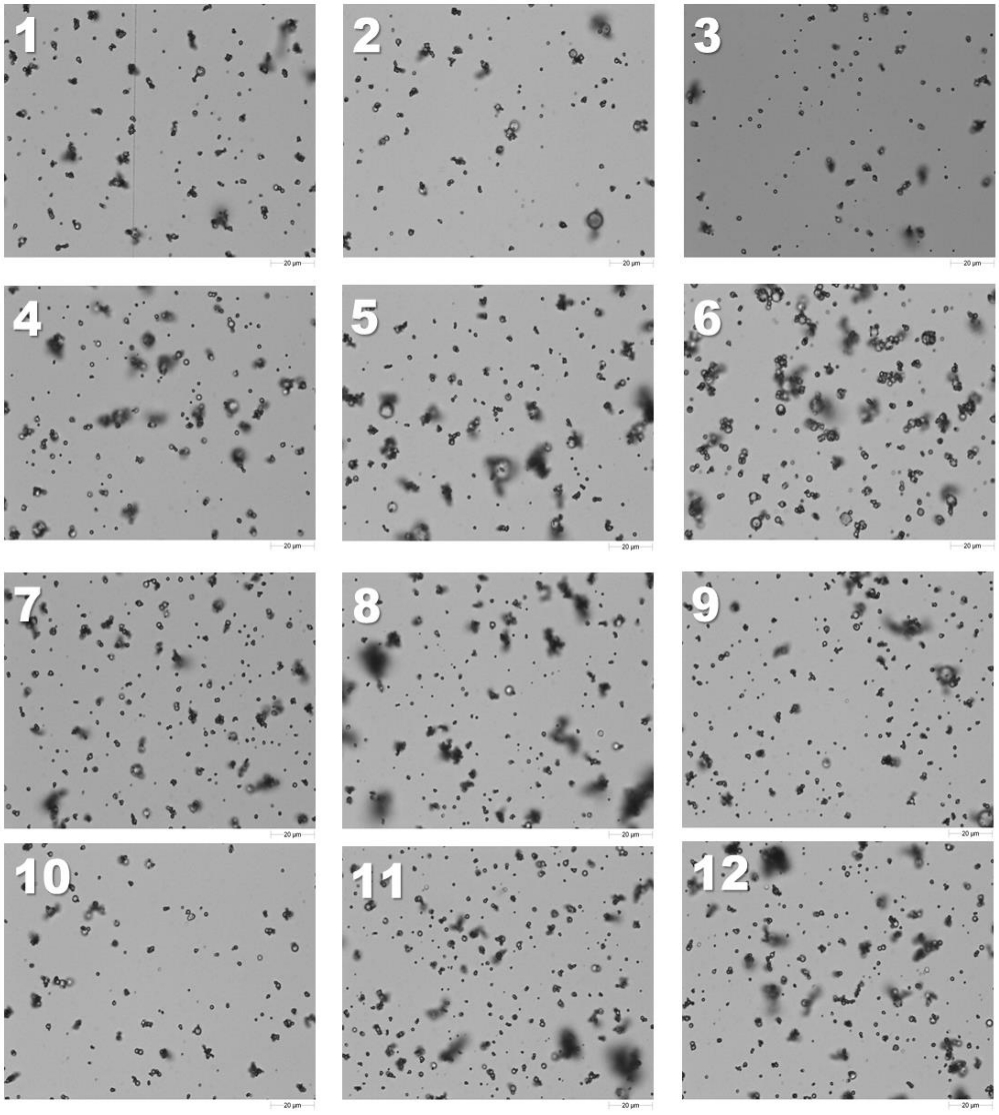

Figure 3.18 Morphologi G3 images of CHT_IBP powders

From the results presented and by analyzing Figure 3.18 and Table 6 it is possible to observe that assay number 5 has the higher respirable fraction and the higher emitted fraction. In terms of FPF the differences between all the assays are not significant, therefore assay 5 conditions were chosen as the best operating conditions. These results are in agreement with CHT itself, discussed earlier. However, it is possible to observe a positive difference between CHT assays and CHT_IBP assays, which means that IBP improves the powder properties, both aerodynamic and morphological.

Table 7 Moisture content and morphological chatacterization of assay 5 from both CHT and CHT_IBP

Sample	$D_{v,50}$ (um)	Span	Moisture Content (%)
CHT (assay 5)	4.5	1.0	11.1
CHT_IBP (assay 5)	3.4	1.0	9.7

$D_{v,50}$ – mean volume diameter; **Span** – $(D_{v90} – D_{v10})/D_{v50}$

3. 3 Characterization of the CHT_Fe@Au_OEtOx-SH particles

After finding the best conditions to perform an assay, two different formulations containing the nanoparticles were engineered: one with a model drug, IBP, and another one without the model drug, CHT_Fe@Au_OEtOxSH_IBP and CHT_Fe@Au_OEtOx-SH, respectively.

The particles were produced using a solution containing 1% (w/v) of CHT in 100 mL of acidic water and ethanol (60:25). To this solution were added 15 mL (7.311 mg) of the nanoparticles. The particles were characterized in terms of morphology via Morphologi G3 equipment; aerodynamic performance, via ACI assays; chemical properties, via FT-IR analysis; solid state, via XRD and BET analyses; and moisture content, via Karl Fischer Coulometric Titration method. The entrapment efficiency (E%) was also calculated in order to understand the amount of nanoparticles that were entrapped in the CHT microspheres.

Table 8 – Powders physical characteristics. ND – Not detectable.

Sample	$D_{v,50}$ (µm)	Span	Moisture Content (%)	Entrapment Efficiency (%)	Surface Area (m^2/g)	Pore Volume (cm^3/g)	Pore size (nm)
CHT	3.5	1.0	11.1	-	15.6 ± 0.8	4.2	6.3
CHT_Fe@Au_ OEtOx-SH	2.9	0.8	11.7	71.7	7.9	ND	ND

$D_{v,50}$ – mean volume diameter; **Span** – $(D_{v90} – D_{v10})/D_{v50}$

From Table 8 it is possible to verify that both formulations present a volumetric diameter around the 3 µm, which allows these particles to efficiently deposit in the deep lung region. Karl Fisher assay allowed the assessment of particles moisture content, which was found to be in the range of 11.1 – 11.7 % for the engineered formulations. This relatively small moisture content of these particles allowed them to efficiently swell when in contact with the lung mucosa, and therefore release both nanoparticles and drug in a controlled and sustained manner.

The results obtained for BET specific surface area analysis are also shown in Table 8. However, due to its heterogeneity it was not possible to measure CHT_Fe@Au_OEtOx-SH pore size neither pore volume.

Also, analyzing Morphologi G3 and SEM images, Figures 3.19 and 3.20, respectively, it is possible to verify that particles present a spherical shape with smooth to rough surfaces and even some distorted spheres.

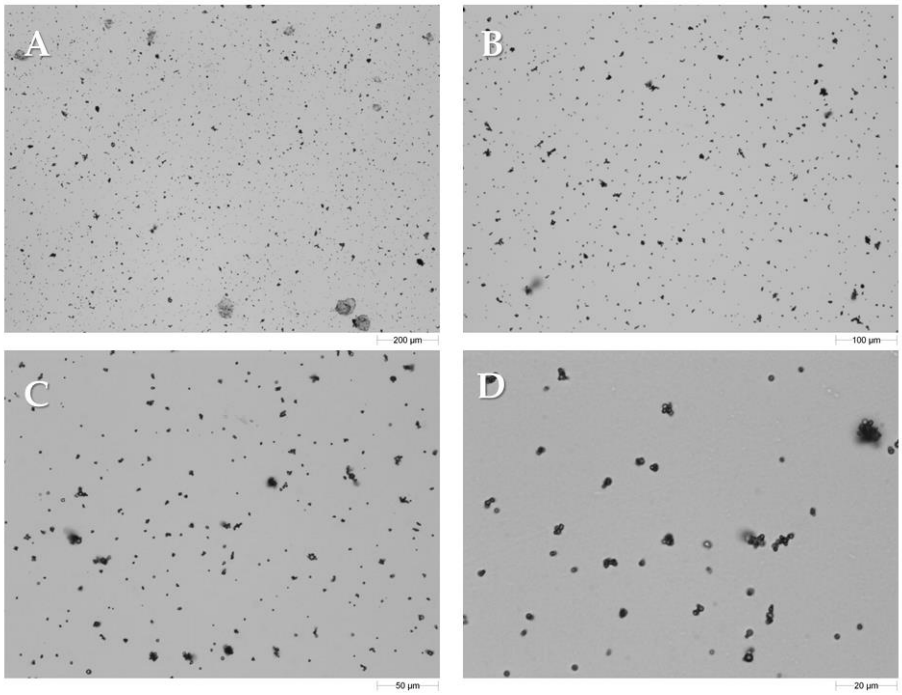

Figure 3.19 Morphologi G3 images of CHT_Fe@Au_OEtOx-SH powders at different magnifications: a) 5x, b) 10x, c) 20x, d) 50x.

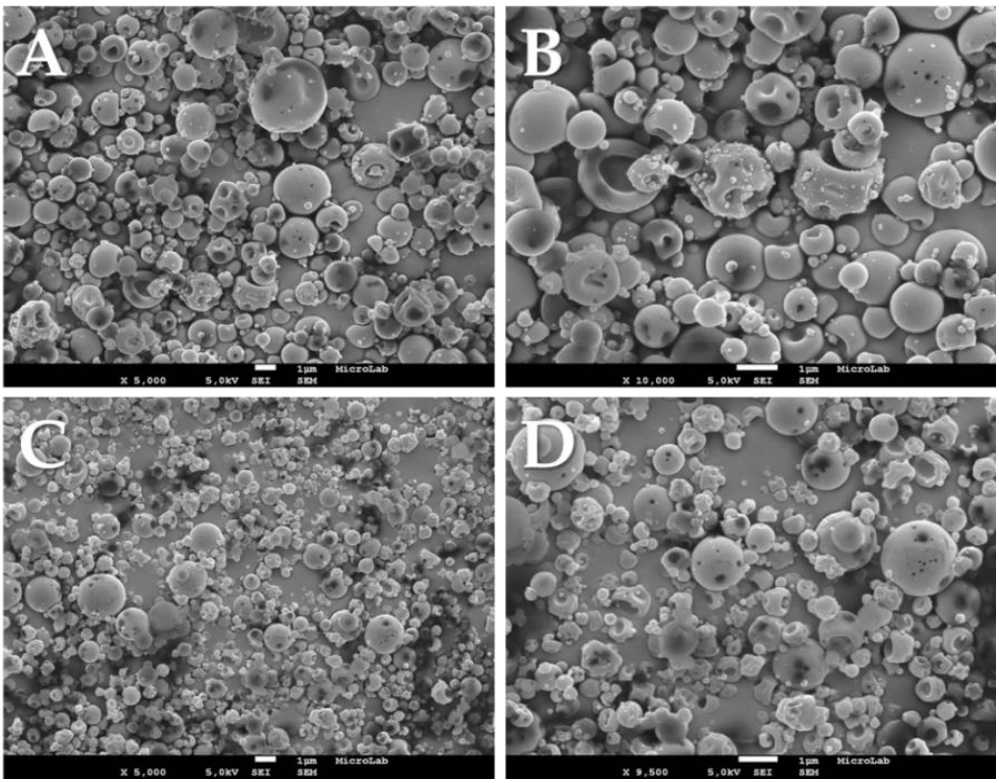

Figure 3.20 SEM images of A and B – CHT; C and D – CHT_Fe@Au_OEtOx-SH

In order to evaluate particles aerodynamic performance, the ACI analysis was performed. Two different assays were performed: one combining the nano-in-micro formulations using a magnet in the end of the ACI (stage 6) and another one combining the same formulation, but without a magnet. This experiment was performed in order to verify if there were any differences when applying a magnetic field. The results are displayed in Table 9 and Figure 3.19.

Table 9 Aerodynamic properties of CHT_Fe@Au_OEtOx-SH powders using a magnet and without using a magnet

Assay	MMAD (μm)	RF (%)	FPF (%)	GSD (%)	EF (%)	Yield, η (%)
Magnet	1.2 ± 0.1	82.6 ± 0.5	55.4 ± 2	3.3 ± 0.5	99.4 ± 0.1	38
No Magnet	1.5 ± 0.1	70.2 ± 0.3	55 ± 2	2.5 ± 0.1	97.5 ± 0.04	38

MMAD – Mass Median Aerodynamic Diameter; **RF** – Respirable Fraction; **FPF**- Fine Particle Fraction; **GSD** – Geometric Standard Deviation; **EF** – Emitted Fraction

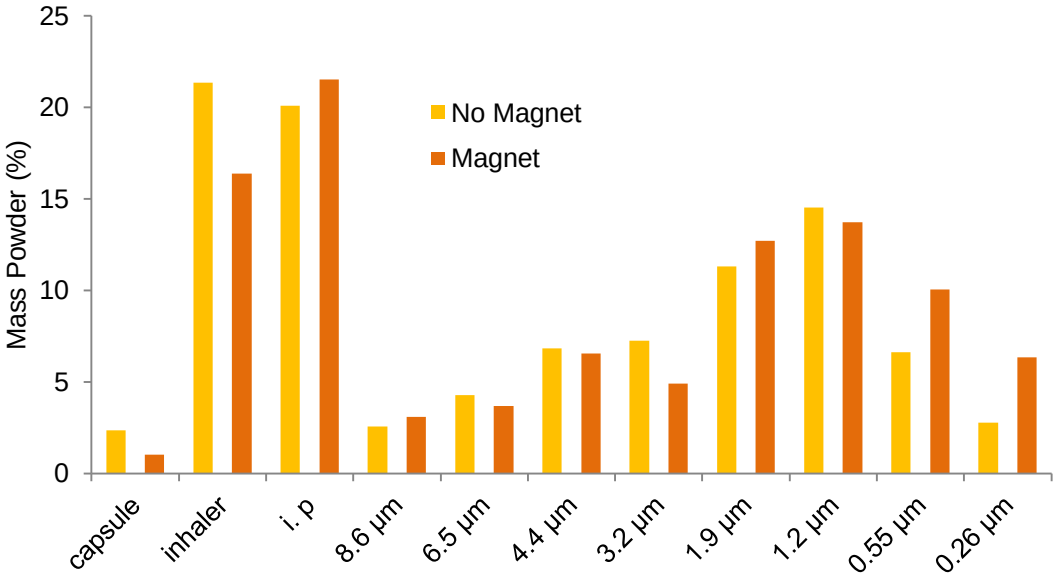

Figure 3.21 Representation of the particles distribution (with and without a magnet) troughout the different stages of the ACI. I.p stands for induction port.

Figure 3.21 shows that when using a magnet in the end of the ACI, particles have a tendency to deposit more in that stage. This effect can be caused by the applied magnetic field in such stage; however, in order to confirm this, more studies should be performed to prove that this difference is specifically related to the magnetic field applied and not to other factor.

An ACI study was also executed to compare if there were any differences between CHT microparticles and CHT microparticles with NPs. As already mentioned in the introductory section, for microparticles to successfully reach the deep lung, particles should have sizes ranging from 1 and 5 µm aerodynamic diameters, to be able to pass through the mouth, throat and conducting airways. If the particles are larger than 5 µm they will be trapped in the upper airways. On the other hand, if they are below 1µm they are exhaled and fail to deposit.

The percentage of particle deposition on each stage of ACI, adapter, capsule and the device was calculated and the emitted fraction of all formulations was also determined. For all microparticles, the emitted fraction obtained was above 96 % indicating that almost all of the powder is released from the capsule. In Figure 3.21 it is possible to verify that the majority of the powder was lost in the induction port, which simulates the upper airways and in the inhaler. This may be due to the formation of turbulent eddies in this zone and the major particles aggregates cannot reach further stages, and to static electricity, respectively.

Table 10 Aerodynamic properties of CHT and CHT_Fe@Au_OEtOx-SH formulations.

Assay	MMAD (µm)	RF (%)	FPF (%)	GSD (%)	EF (%)
CHT	1.2 ± 0.2	65 ± 2	48 ± 2	3.4 ± 0.3	96.3 ± 0.1
CHT_Fe@Au_OEtOxSH	1.5 ± 0.1	70.2 ±0.3	55 ± 2	2.5 ± 0.1	97.50 ± 0.04

MMAD – Mass Median Aerodynamic Diameter; **RF** – Respirable Fraction; **FPF**- Fine Particle Fraction; **GSD** – Geometric Standard Deviation; **EF** – Emitted Fraction

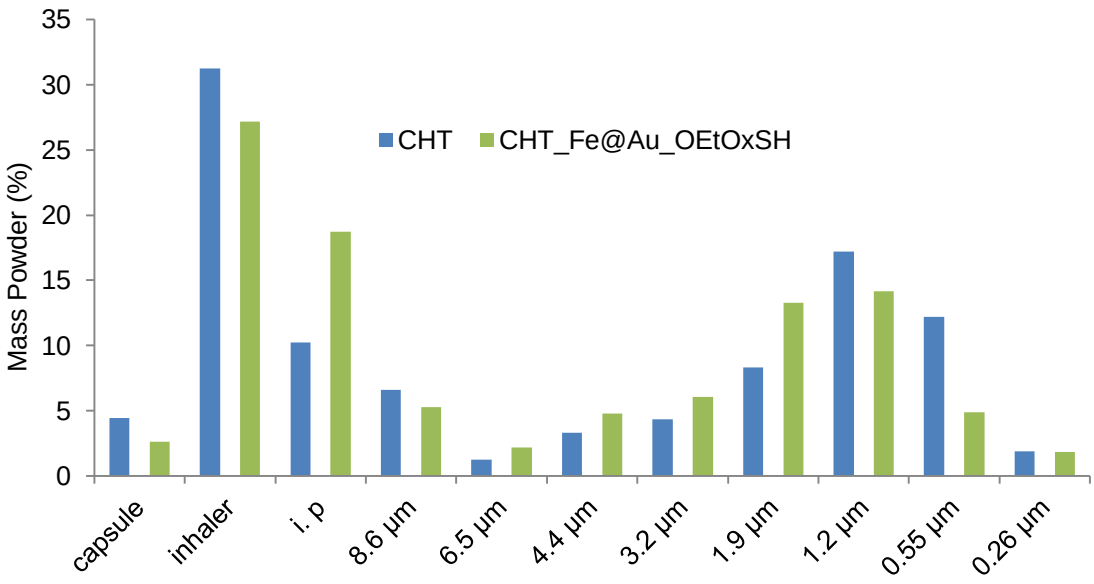

Figure 3.22 Representation of particles distribution throughout the different stages of the ACI.

As shown in Table 10, the formulations have different MMAD and FPF; but both are able to deposit a large amount of particles in the deep lungs. As demonstrated, FPF is improved with the addition of the nanoparticles, turning from 49 to 55%, thus these powders have a substantial mass fraction of particles below 5 µm, able to reach the deep lungs.

Fe@Au nanoparticles formulations into CHT microspheres appear to influence the aerodynamic performance of the microparticles. The percentage of particles reaching the latest stages of ACI is higher when adding nanoparticles than CHT alone. The improved aerodynamic performance of formulations comprising Fe@Au NPs might be due to their higher stability and lower surface energy.

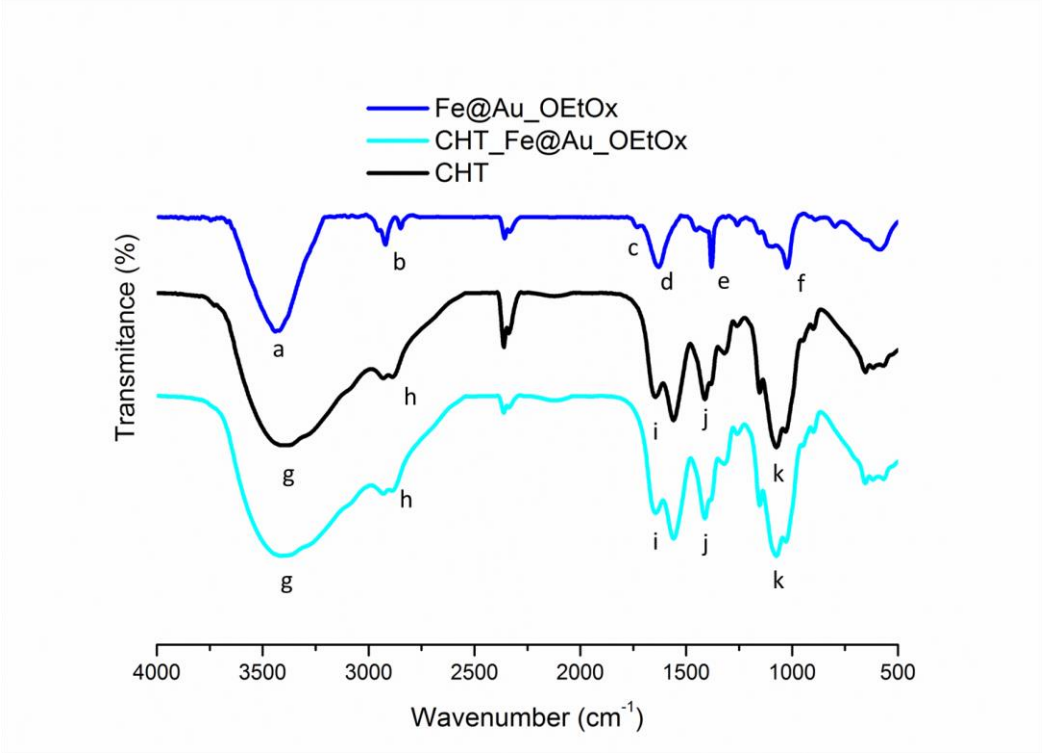

Figure 3.23 FT-IR spectra of the nanoparticles and CHT formulations

Analysing Figure 3.23 there are some characteristic bands of OEtOx-SH polymer and CHT powders. Around the 3500 cm^{-1} it is possible to see a O-H stretch from the polymer (**a – 3436 cm^{-1}**) and from CHT (**g – 3415 cm^{-1}**); at ≈ 2900 cm^{-1}, the characteristic band of C-H stretches (**b – 2923 cm^{-1}** and **h – 2894 cm^{-1}**); Et(C=O)N stretch from OEtOX-SH can be found around 1700 cm^{-1} (**c – 1715 cm^{-1}** and **d – 1693 cm^{-1}**);at approximately 1000 cm^{-1} it is possible to see a C-N stretch of the tertiary amine from Au_OEtOx-SH bonding (**f – 1069 cm^{-1}**) and a C-O stretch of CHT structure (**k – 1076 cm^{-1}**) ; between 1600 and 1650 cm^{-1} an N-H bend from the amine groups of CHT is found (**i – 1645 cm^{-1}**); C-H bend from CH_3 is found at 1400 cm-1, either from OEtOx-SH and CHT (**e – 1406 cm^{-1}** and **j – 1409 cm^{-1}**).

Also, it is possible to understand that due to the high amount of CHT in relation to the amount of nanoparticles, there are no significant changes between CHT and CHT_Fe@Au_OEtOx-SH formulations.

The XRD patterns of CHT and CHT_Fe@Au_OEtOxSH are displayed in Figure 3.24. Both formulations only exhibit the amorphous state of processed CHT (broadening at 2θ =20º). IBP XRD pattern has already been analyzed in the literature revealing the presence of sharp peaks, confirming its crystalline structure.[32,102] Likewise, magnetic nanoparticles are also described in the literature as crystalline nanoparticles.[103,104] Upon co-atomization with CHT, no crystalline peaks are denoted, corroborating that our particles are fully entrapped in the CHT

matrix. Such amorphous excipients are able to stabilize the active pharmaceutical ingredient (API), increasing the dissolution rate. Moreover, these excipients show a high water adsorption capacity, contributing for a sustained release and a fast cellular absorption. The API, on the other hand, should be in a crystalline form in order to maintain its bioavailability, maximizing its efficiency and reducing the required dosage. [18]

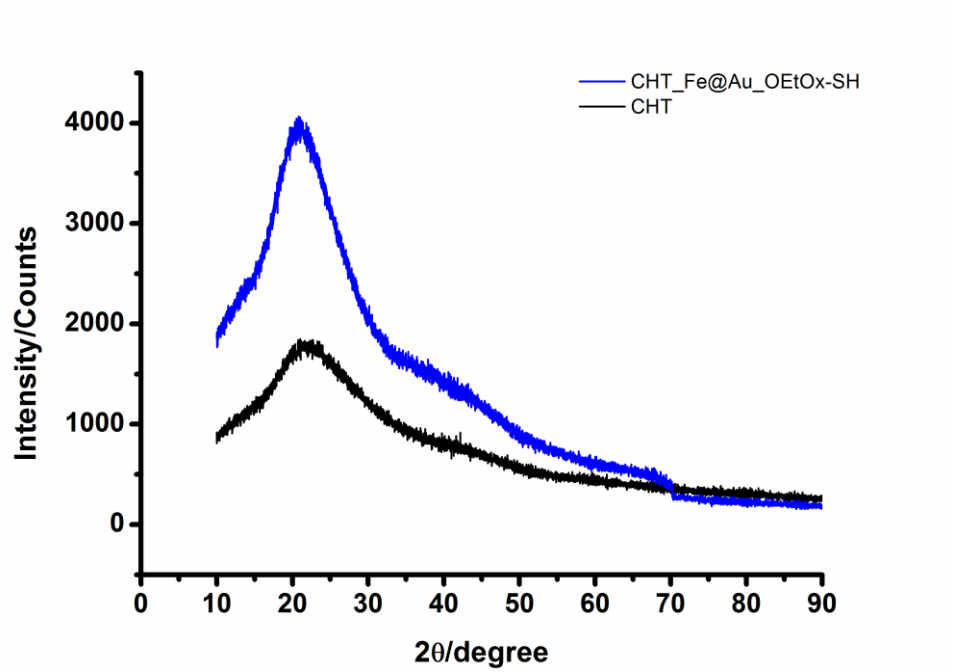

Figure 3.24 XRD pattern of CHT and CHT_Fe@Au_OEtOx_SH

To study the release of the nanoparticles from the microspheres, two release studies were performed to evaluate the release profile. Both studies were carried in two different pHs, mimmetizing the conditions of a healthy lung (pH 7.4) and a cancerous lung (pH 6.8). The first one was set in order to study if there was any magnetism when the nanoparticles were released from CHT. For this, a magnet was placed under both solutions and the photos were acquired.

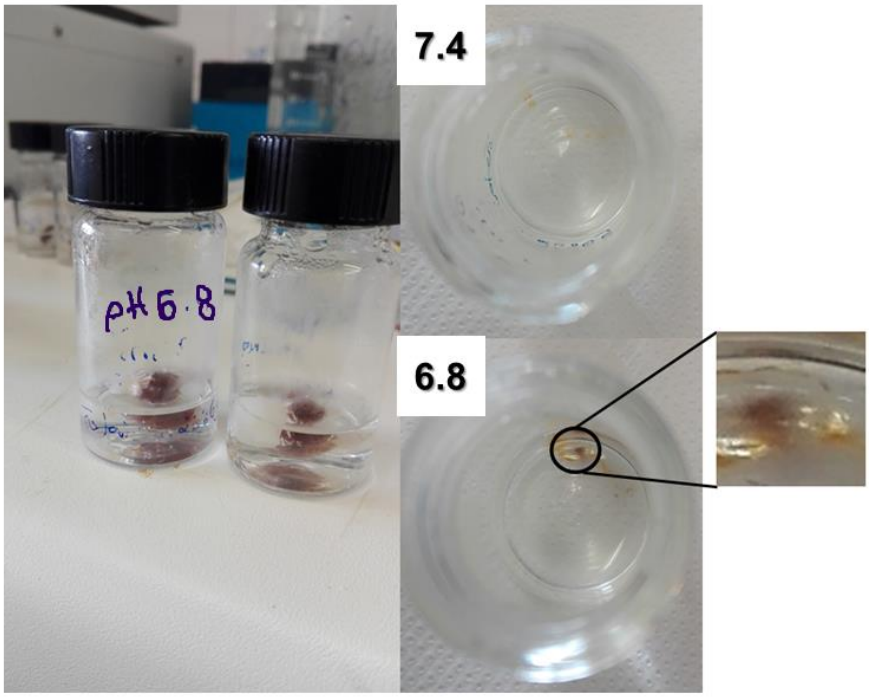

Figure 3.25 - Release study of the nanoparticles from the microparticles using a magnet. Figure on the left shows the flasks containing the powders in different pH solutions.

It is possible to observe a small black dot in the solution of pH 6.8 (Figure 3.25), exactly where the magnet was located. This is indicative that when released from CHT, nanoparticles still maintain their magnetism, which allows them to deposit in a place where a magnetic field is being applied. These results demonstrate, as a proof-of-concept the feasibility to encapsulate magnetic nanoparticles for inhalation. However, further studies should be performed in order to understand the ideal force of an induced magnetic field that need to be applied in a real situation.

3.4 Characterization of CHT_Fe@Au_OEtOxSH_IBP particles

To the already known system of CHT_Fe@Au_OEtOxSH particles, a model drug was attached in order to see if there were any significant changes in terms of morphological and aerodynamic properties. Also, this model drug was encapsulated to evaluate this system in terms of controlled release. Therefore, an *in vitro* cumulative release study was performed, and this was adjusted to the Korshmeyer-Peppas mathematical model. Solutions containing 1% (w/v) of CHT in a volume of 100 mL (60% acidic water, 25% Ethanol and 15% NPs solution) were prepared and then 100 mg of Ibuprofen was added.

Table 11 Physical properties of CHT_Fe@Au_OEtOxSH_IBP particles

Sample	$D_{v,50}$ (um)	Span	Moisture Content (%)	Entrapment Efficiency (%)
CHT_Fe@Au_OEtOXSH_IBP	3.127	0.98	10	68.33

$D_{v,50}$ – mean volume diameter; **Span** – $(D_{v90} – D_{v10})/D_{v50}$

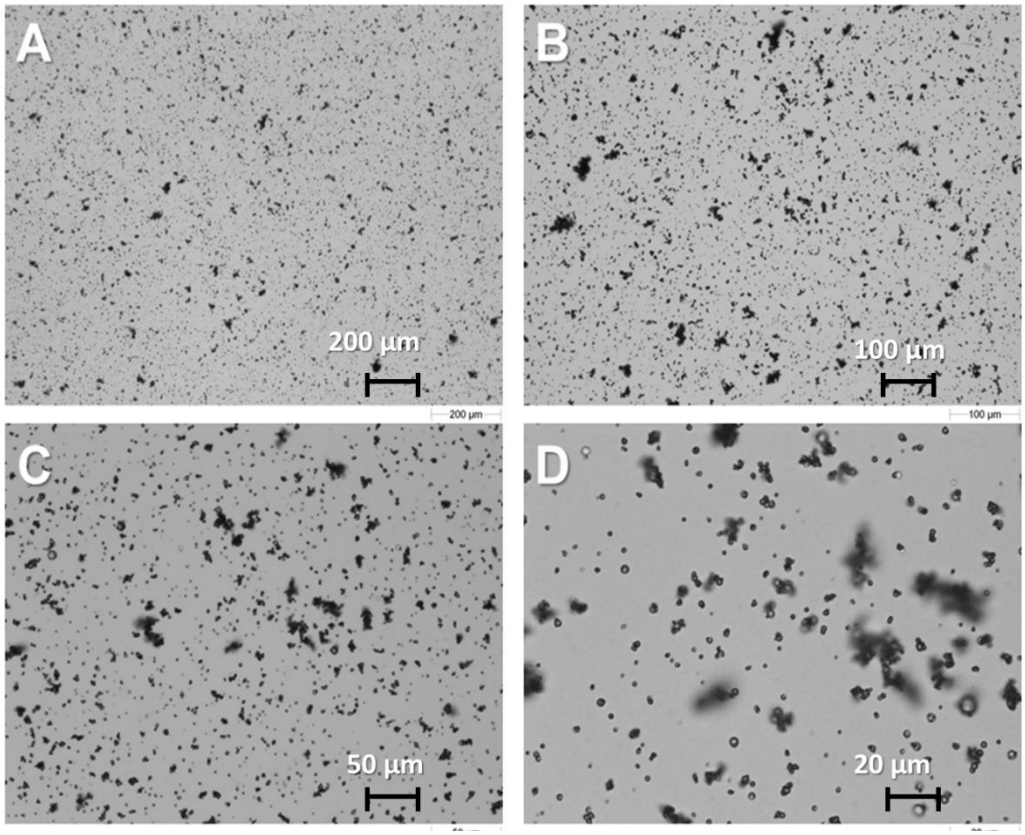

Figure 3.26 Morphologi G3 images of CHT_Fe@Au_OEtOx-SH_IBP formulations

ACI results of the solutions with Ibuprofen are presented in Table 12. As seen, and comparing with the results displayed in the last section, the addition of IBP to CHT microparticles and the addition to CHT_Fe@Au_OEtOxSH microparticles, have improved both FPF and EF results. When comparing CHT with CHT_IBP, a significant change in FPF is visible, once it changes from 49 to 54%. The same happened to the amount of respirable particles (RF) which is also increased by the addition of IBP: from 65 to 72% in the case of CHT, and from 70 to 75% in the case of CHT_Fe@Au_OEtOxSH. When comparing the EF in both cases, it is possible to observe, as well, an increment of the values when adding IBP. In the case of CHT and CHT_IBP, EF changes from 96.3 to 97.5%.

By analyzing the data it is possible to conclude that IBP confers greater aerodynamic properties to this system, indicating that by attaching a drug to it, the aerodynamic conditions are not negatively affected and proving that it can be used as a drug delivery system.

Table 12 Aerodynamic properties of CHT_Fe@Au_OEtOx-SH_IBP formulation

Assay	MMAD (µm)	RF (%)	FPF (%)	GSD (%)	EF (%)
CHT_IBP	1.3 ± 0.2	72.1 ± 2.8	53.5 ± 2.8	1.9 ± 0.1	97.5 ± 0.8
CHT_Fe@Au_OEtOxSH_IBP	1 ± 0.1	74.8 ± 2	55.8 ± 1.2	2.5 ± 0.1	98.7 ± 0.2

MMAD – Mass Median Aerodynamic Diameter; **RF** – Respirable Fraction; **FPF**- Fine Particle Fraction; **GSD** – Geometric Standard Deviation; **EF** – Emitted Fraction

By comparing only CHT_IBP to CHT_Fe@Au_OEtOxSH_IBP it is possible to observe that all the values are very similar. Thus, the changes analyzed above are most certainly due to the addition of IBP and not to the addition of NPs. As seen in Figure 3.27 both the formulations of CHT_IBP and CHT_Fe@Au_OEtOxSH_IBP are able to reach the final stages of the ACI, indicating that these formulations are also able to deposit in the deep lung region. Also, particles tend to accumulate in the inhaler and in the induction port, this is also justified by the static electricity and by the formation of turbulent eddies in the upper airways (induction port).

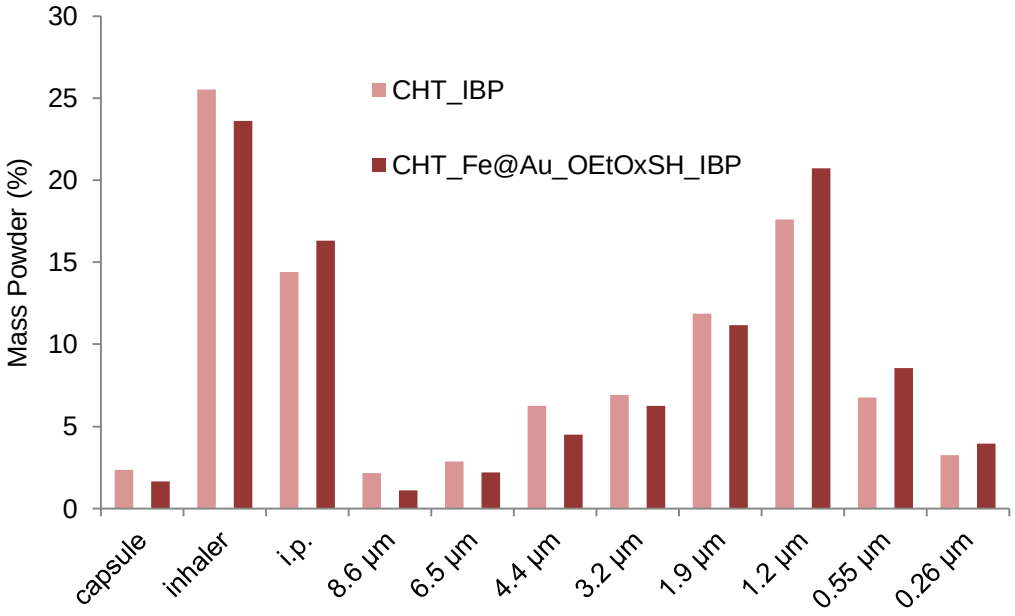

Figure 3.27 Representation of particle distribution throughout the different stages of the ACI

To evaluate the release profile of IBP from the nano-in-micro formulations, a study was carried in two different pHs, mimetizing the conditions of a healthy lung (pH 7.4) and a cancerous lung (pH 6.8). As previously mentioned, the release profile was adjusted to Korsmeyer-Peppas mathematical model.

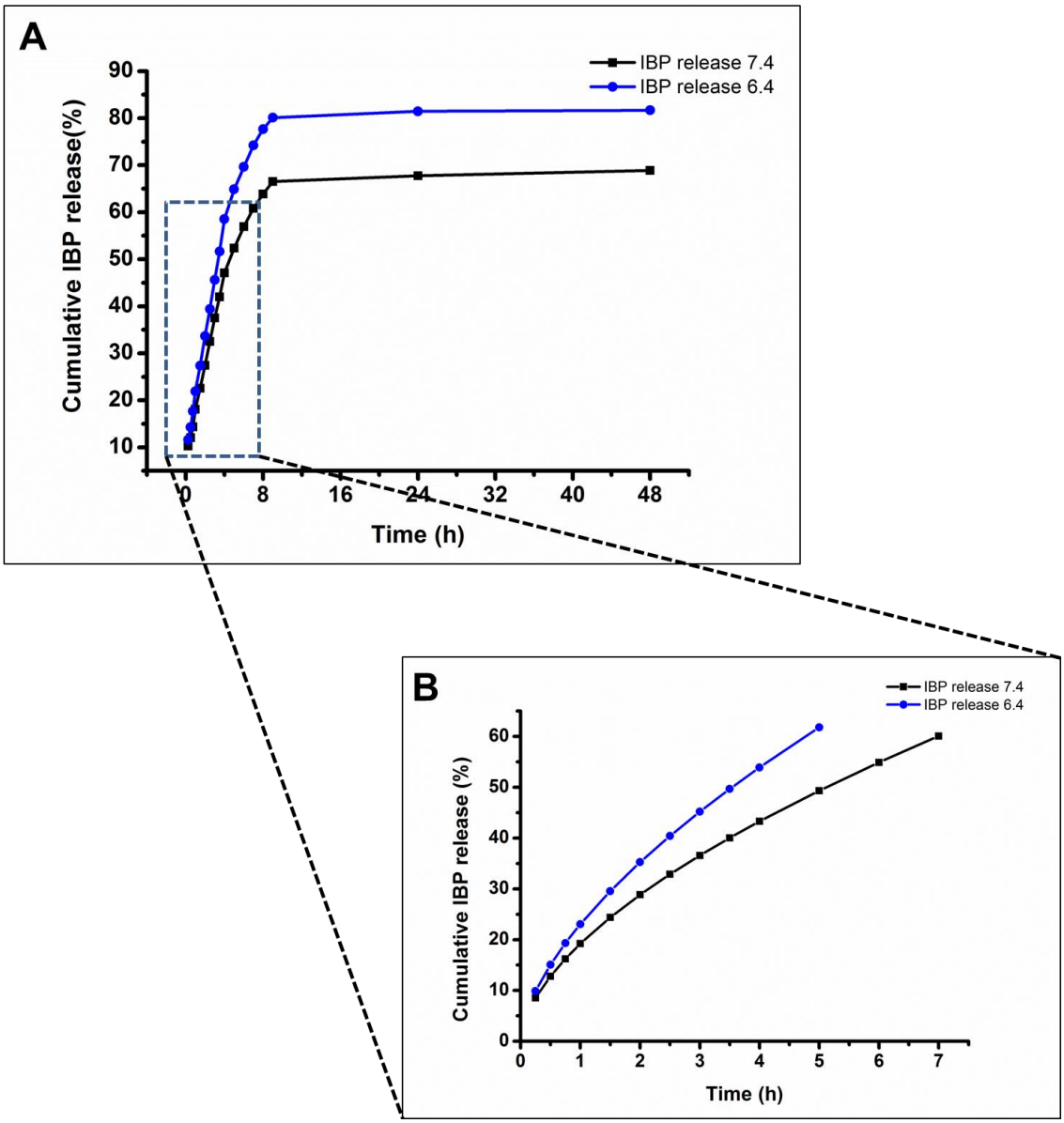

Figure 3.28 A) *In vitro* cumulative release studies at different pHs; B) Korsmeyer-Peppas adjustment for 60% of the release

Table 13 Korsmeyer-Peppas adjustment values for IBP release

	n	**k (h^{-1})**	**% mass released**
pH 7.4	0.6	23.1	68.9
pH 6.8	0.6	19.2	81.7

n – diffusional exponent; **k** – constant

As depicted in the Figure 3.28, the release profile of IBP is different in the two pHs. The n-value is obtained from the slope of the Korsmeyer-Peppas plot and represents different release mechanisms. For spherical geometries: n=0.43 for Fickian diffusion; 0.43<n<0.85 for anomalous non-Fickian diffusion; n=0.85 for Case-II transport. Therefore, in both cases, the n-value is 0.6, which means that we are in the presence of a non-Fickian diffusion. Having an anomalous transport the release rate has the contribution of both diffusion and relaxational mechanisms-stresses during polymer swelling.

As seen, the amount of released particles is higher at pH 6.8 than pH 7.4. This occurs since the pKa of CHT is around 6.5, thus at 6.8 CHT has approximately half of its amino groups are protonated turning the matrix more hydrophilic than at pH 7.4 where the amino groups are deprotonated. This leads to a faster release of IBP from the CHT particles at pH 6.8 than at 7.4.

These results also show us that this system is capable of releasing a drug in a controlled manner and that it could easily release IBP in a lung cancer situation (pH 6.8), therefore conferring great outcomes for the release of a drug in an unhealthy condition.

4

Conclusions

In the present work, CHT microparticles containing the functionalized NPs and IBP were successfully micronized. These powders exhibit appropriate characteristics, either in terms of their size, morphology or aerodynamic properties, all suitable for inhalation. CHT has also proved to be a potential candidate to be used as carrier for therapeutic agents in a lung cancer situation since it has a higher release percentage at an acidic pH condition (cancerous pH). As presented in the introduction, the development of dry powders for inhalation stands as an outbreak solution to overcome drawbacks associated with drug delivery. Herein, we have proved that this system is capable to overcome these problems. The fluorescent and magnetic nanoparticles can be used in lung cancer imaging and hyperthermia. However further studies concerning the use of an applied magnetic field should be made in order to prove their efficacy. Although we have proven that the final NPs presented fluorescence due to the presence of the oligo(2-oxazoline), it is necessary to perform a confocal laser microscopy study to prove their effectiveness towards imaging. Also, as demonstrated in the release studies conducted with a magnet and from the ACI studies performed with a magnet as well, we have seen that the NPs still maintain their magnetism, especially after being released from the microspheres. Therefore, in order to understand if this system can be used as imaging, by making use of the magnetic core, a magnetic resonance imaging (MRI) experiment should also be assessed. Magnetic hyperthermia studies in lung cancer cells are also needed to prove that these NPs are able to kill a lung cancer cell by heating and vibrating the nanoparticles.

Based on their sizes and zeta potential, as well as fluorescent capabilities, the developed NPs should be in suitable conditions for appropriate cellular internalization and imaging. *In vitro* cellular experiments should be conducted in order to sustain the theory. If the results are favorable, moving to an *in vivo* scale should be the next step. The idea is to be able to conduct particles, with the aid of their magnetic field, to an exact location like the cancerous tissue, as seen in Figure 4.29.

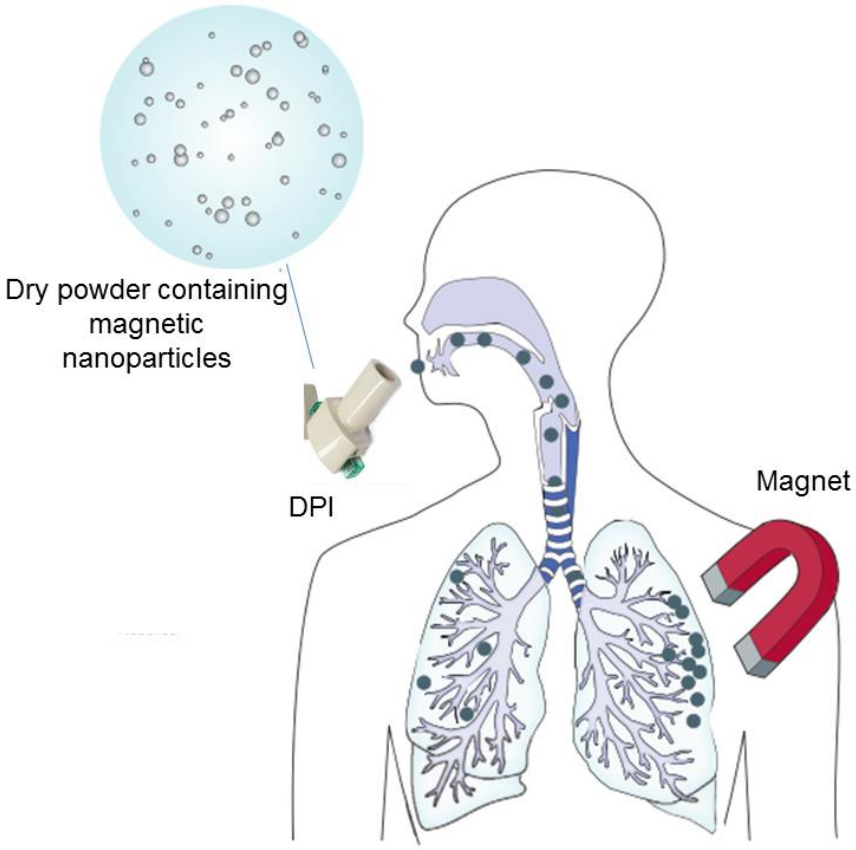

Figure 4.29 Schematic representation of the delivery of a dry powder contain magnetic nanoparticles in order to guide them to the desired region(s) of the lung by using of a strong external magnetic field. Adapted from M. Dolovich et al. [105]

Regarding the SASD apparatus, an optimization process was engineered for this project in order to increase the recovery yields. Temperatures were increased, improving process yields from 20 to 70-80 %. Further optimizations regarding the pressure should also be conducted. Despite the great increase in the percentage of recovered particles, a significant percentage is being lost during the process by leaving with the gas stream. Thus, it is necessary to come up with a strategy, like the use of filters, capable of trapping these particles, in the recovery flask. The production of CHT microparticles should also be optimized in order to create less aggregated particles. For this, a deeper study (besides DoE) concerning pressures and temperatures during the process should be addressed.

DoE studies enabled us to understand which were the best operating conditions when working with formulations containing CHT and CHT with IBP. In both cases, at higher pressures and higher flows, the obtained results were improved, either in terms of respirable fractions as in terms of fine particle fraction. After choosing the best operating conditions, the assays containing the NPs and IBP were performed. Both the powders presented suitable aerodynamic

and morphological characteristics, and the assay containing IBP showed an 80% release during 48 hours of study. This indicates us that this system is not only able to deposit in the deep lung region, but also to release a drug in a controlled manner. Although particles did not show any reaction upon the application of a magnetic field, there were slightly changes in the ACI studies with and without the magnet. This is indicative that the powders may have magnetism, even if it is at a small percentage. To confirm these preliminary results, replicates should be performed in order to evaluate its statistical significance. Also, when we performed the release study of the NPs with the magnet, it was possible to verify that a small dot of NPs tend to deposit on the place where the magnet was. This may lead us to the idea that the NPs actually maintain their magnetism, although some of it is lost when covering the nanoparticles with CHT.

To conclude, the system developed along this project is a possible candidate for pulmonary administration of drugs either for local or systemic theragnosis. Although, as referred earlier, these studies are insufficient to determine that this is in fact a viable system, the proof of concept studies are satisfactory as it demonstrated the feasibility of the process for the production of an adequate drug delivery system for pulmonary use in lung cancer situations.

5

References

1. Sanders, M. in *Controlled Pulmonary Drug Delivery* 51–73 (2011). doi:10.1007/978-1-4419-9745-6
2. Bailey, M. M. & Berkland, C. J. Nanoparticle formulations in pulmonary drug delivery. *Medicinal Research Reviews* **29,** 196–212 (2009).
3. Buttini, F., Colombo, P., Rossi, A., Sonvico, F. & Colombo, G. Particles and powders: Tools of innovation for non-invasive drug administration. *J. Control. Release* **161,** 693–702 (2012).
4. Xu, W., Ling, P. & Zhang, T. Polymeric micelles, a promising drug delivery system to enhance bioavailability of poorly water-soluble drugs. *J. Drug Deliv.* **2013,** 340315 (2013).
5. Sarasija, S. & Patil, J. Pulmonary drug delivery strategies: A concise, systematic review. *Lung India* **29,** 44–50 (2012).
6. Takami, T. & Murakami, Y. Development of PEG-PLA/PLGA microparticles for pulmonary drug delivery prepared by a novel emulsification technique assisted with amphiphilic block copolymers. *Colloids Surfaces B Biointerfaces* **87,** 433–438 (2011).
7. Begat, P., Morton, D. A. V, Staniforth, J. N. & Price, R. The cohesive-adhesive balances in dry powder inhaler formulations I: Direct quantification by atomic force microscopy. *Pharm. Res.* **21,** 1591–1597 (2004).
8. Shaikh, Siraj; Nazim, Sayyed; Khan, Tarique; Shaikh, Afsar; Zameerudinni, M. & Quazi, A. Recent Advances in Pulmonary Drug Delivery Systems: A Review. *Int. J. Appl. Pharm.* **2,** 27–34 (2010).
9. Patel, Ashaben; Patel, Mitesh; Yang, Xiaoyan; Mitra, A. K. Recent Advances in Protein and Peptide Drug Delivery - A Special Emphasis on Polymeric Nanoparticles. *Protein Pept. Lett.* **21,** 1102–1120 (2014).
10. Sung, J. C., Pulliam, B. L. & Edwards, D. A. Nanoparticles for drug delivery to the lungs. *Trends Biotechnol.* **25,** 563–570 (2007).
11. Pilcer, G. & Amighi, K. Formulation strategy and use of excipients in pulmonary drug delivery. *Int. J. Pharm.* **392,** 1–19 (2010).
12. Newman, S. P. & Busse, W. W. Evolution of dry powder inhaler design, formulation, and

performance. *Respiratory Medicine* **96,** 293–304 (2002).

13. Uhrich, K. E., Cannizzaro, S. M., Langer, R. S. & Shakesheff, K. M. Polymeric systems for controlled drug release. *Chem. Rev.* **99,** 3181–98 (1999).

14. Tsifansky, M. *et al.* Microparticles for inhalational delivery of antipseudomonal antibiotics. *AAPS J.* **10,** 254–260 (2008).

15. Wu, X., Hayes, D., Zwischenberger, J. B., Kuhn, R. J. & Mansour, H. M. Design and physicochemical characterization of advanced spray-dried tacrolimus multifunctional particles for inhalation. *Drug Des. Devel. Ther.* **7,** 59–72 (2013).

16. Shoyele, S. A. & Cawthorne, S. Particle engineering techniques for inhaled biopharmaceuticals. *Adv. Drug Deliv. Rev.* **58,** 1009–1029 (2006).

17. Feddah, M. R., Brown, K. F., Gipps, E. M. & Davies, N. M. In-vitro characterisation of metered dose inhaler versus dry powder inhaler glucocorticoid products: influence of inspiratory flow rates. *J. Pharm. Pharm. Sci.* **3,** 318–324 (2000).

18. Chow, A. H. L., Tong, H. H. Y., Chattopadhyay, P. & Shekunov, B. Y. Particle engineering for pulmonary drug delivery. *Pharm. Res.* **24,** 411–437 (2007).

19. Vehring, R. Pharmaceutical particle engineering via spray drying. *Pharmaceutical Research* **25,** 999–1022 (2008).

20. Amidi, M. *et al.* Preparation and physicochemical characterization of supercritically dried insulin-loaded microparticles for pulmonary delivery. *Eur. J. Pharm. Biopharm.* **68,** 191–200 (2008).

21. Smyth, Hugh D C; Hickey, A. J. Carriers in Drug Powder Delivery. *J. Drug Deliv.* **3,** 117–132 (2005).

22. Knez, Z. & Weidner, E. Particles formation and particle design using supercritical fluids. *Curr. Opin. Solid State Mater. Sci.* **7,** 353–361 (2003).

23. Nykamp, G., Carstensen, U. & Müller, B. W. Jet milling--a new technique for microparticle preparation. *Int. J. Pharm.* **242,** 79–86 (2002).

24. Maa, Yuh-Fun; Nguyen, Phuong-Anh; Sweeney, Theresa; Shire, Steven J; Hsu, C. C. Protein Inhalation Powders: Spray Drying vs Spray Freeze Drying. *Pharm. Res.* **16,** 246–254 (1999).

25. Fukushima, Y. Application of Supercritical Fluids. *R&D Rev. Toyota CRDL* **35,** 1–9 (1978).

26. Adami, R., Liparoti, S. & Reverchon, E. A new supercritical assisted atomization configuration, for the micronization of thermolabile compounds. *Chem. Eng. J.* **173,** 55–61 (2011).

27. Sihvonen, M., Järvenpää, E., Hietaniemi, V. & Huopalahti, R. Advances in supercritical carbon dioxide technologies. *Trends in Food Science and Technology* **10,** 217–222 (1999).

28. Della Porta, G., De Vittori, C. & Reverchon, E. Supercritical assisted atomization: a novel technology for microparticles preparation of an asthma-controlling drug. *AAPS PharmSciTech* **6,** E421–E428 (2005).

29. Rahimpour, Y. & Hamishehkar, H. Lactose engineering for better performance in dry powder inhalers. *Adv. Pharm. Bull.* **2,** 183–187 (2012).

30. Reverchon, E., Adami, R. & Caputo, G. Supercritical assisted atomization: Performance comparison between laboratory and pilot scale. *J. Supercrit. Fluids* **37,** 298–306 (2006).

31. Jagannathan, P. E. United States Patent - Process for the production of micro and/or nano particles. **2,** (2010).

32. Cabral, R. P. *et al.* Design of experiments approach on the preparation of dry inhaler

chitosan composite formulations by supercritical CO2-assisted spray-drying. *J. Supercrit. Fluids* **116,** 26–35 (2016).

33. Reverchon, E. & Antonacci, A. Chitosan microparticles production by supercritical fluid processing. *Ind. Eng. Chem. Res.* **45,** 5722–5728 (2006).

34. Duarte, C., Aguiar-Ricardo, A., Ribeiro, N., Casimiro, T. & Da Ponte, M. N. Correlation of Vapor–Liquid Equilibrium for Carbon Dioxide + Ethanol + Water at Temperatures from 35 to 70°C. *Sep. Sci. Technol.* **35,** 2187–2201 (2000).

35. Li, J., Rodrigues, M., Matos, H. A. & Azevedo, E. G. De. VLE of Carbon Dioxide/Ethanol/Water: Applications to Volume Expansion Evaluation and Water Removal Efficiency. *Carbon N. Y.* **44,** 6751–6759 (2005).

36. Reverchon, E. & Della Porta, G. Particle Design Using Supercritical Fluids. *Chem. Eng. Technol.* **26,** 840–845 (2003).

37. Gallo, L. *et al.* Solubility of carbon dioxide in ternary and quaternary mixtures of water , CO 2 , malic acid and glucose : experimental results and phase equilibrium modeling. *Chem. Eng. Trans.* **17,** 1053–1058 (2009).

38. El-Sherbiny, I. M., McGill, S. & Smyth, H. D. C. Swellable microparticles as carriers for sustained pulmonary drug delivery. *J. Pharm. Sci.* **99,** 2343–2356 (2010).

39. Martonen, T. B., Smyth, H. D. C., Isaacs, K. K. & Burton, R. T. Issues in drug delivery: concepts and practice. *Respir. Care* **50,** 1228–52 (2005).

40. Hickey, A. J., Martonen, T. B. & Yang, Y. Theoretical relationship of lung deposition to the fine particle fraction of inhalation aerosols. *Pharm. Acta Helv.* **71,** 185–190 (1996).

41. El-Sherbiny, I. M. & Smyth, H. D. C. Biodegradable nano-micro carrier systems for sustained pulmonary drug delivery: (I) Self-assembled nanoparticles encapsulated in respirable/swellable semi-IPN microspheres. *Int. J. Pharm.* **395,** 132–141 (2010).

42. Ahsan, F., Rivas, I. P., Khan, M. A. & Torres Su??rez, A. I. Targeting to macrophages: Role of physicochemical properties of particulate carriers - Liposomes and microspheres - On the phagocytosis by macrophages. *Journal of Controlled Release* **79,** 29–40 (2002).

43. H. M. Courrier, N. B. and T. F. V. Pulmonary Drug Delivery Systems: Recent Developments and Prospects. *Crit. Rev. Ther. Drug Carrier Syst.* **19,** 425–498 (2002).

44. Kim, C. *et al.* Cyclodextrin-covered gold nanoparticles for targeted delivery of an anti-cancer drug. *J. Mater. Chem.* **19,** 2261–2440 (2009).

45. Han, G., Ghosh, P. & Rotello, V. M. Functionalized gold nanoparticles for drug delivery. *Nanomedicine (Lond).* **2,** 113–123 (2007).

46. Grenha, A., Remuñán-López, C., Carvalho, E. L. S. & Seijo, B. Microspheres containing lipid/chitosan nanoparticles complexes for pulmonary delivery of therapeutic proteins. *Eur. J. Pharm. Biopharm.* **69,** 83–93 (2008).

47. Barnaby, S. N., Sita, T. L., Petrosko, S. H., Stegh, A. H. & Mirkin, C. A. Nanotechnology-Based Precision Tools for the Detection and Treatment of Cancer. *Cancer Treat. Res.* **166,** 293–322 (2015).

48. Rana, S., Bajaj, A., Mout, R. & Rotello, V. M. Monolayer coated gold nanoparticles for delivery applications. *Advanced Drug Delivery Reviews* **64,** 200–216 (2012).

49. Chatterjee, K., Sarkar, S., Jagajjanani Rao, K. & Paria, S. Core/shell nanoparticles in biomedical applications. *Adv Colloid Interface Sci* **209,** 8–39 (2014).

50. Silva, A. S., Tavares, M. T. & Aguiar-Ricardo, A. Sustainable strategies for nano-in-micro particle engineering for pulmonary delivery. *J. Nanoparticle Res.* **16,** 2602 (2014).

51. Huynh, N. T., Roger, E., Lautram, N., Benoît, J.-P. & Passirani, C. The rise and rise of

stealth nanocarriers for cancer therapy: passive versus active targeting. *Nanomedicine (Lond).* **5,** 1415–1433 (2010).

52. Koo, O. M., Rubinstein, I. & Onyuksel, H. Role of nanotechnology in targeted drug delivery and imaging: a concise review. *Nanomedicine Nanotechnology, Biol. Med.* **1,** 193–212 (2005).

53. Dong, S.-A. & Zhou, S.-P. Photochemical synthesis of colloidal gold nanoparticles. *Mater. Sci. Eng. B* **140,** 153–159 (2007).

54. Jia, Z., Wu, H. & Morbidelli, M. Thermal restructuring of fractal clusters: The case of a strawberry-like core-shell polymer colloid. *Langmuir* **23,** 5713–5721 (2007).

55. Spasova, M. *et al.* Magnetic and optical tunable microspheres with a magnetite/gold nanoparticle shell. *J. Mater. Chem.* **15,** 2095–2098 (2005).

56. Umut, E. *et al.* Magnetic, optical and relaxometric properties of organically coated gold–magnetite (Au–Fe3O4) hybrid nanoparticles for potential use in biomedical applications. *J. Magn. Magn. Mater.* **324,** 2373–2379 (2012).

57. Wahajuddin & Arora, S. Superparamagnetic iron oxide nanoparticles: Magnetic nanoplatforms as drug carriers. *Int. J. Nanomedicine* **7,** 3445–3471 (2012).

58. Gupta, A. K. & Wells, S. Surface-Modified Superparamagnetic Nanoparticles for Drug Delivery: Preparation, Characterization, and Cytotoxicity Studies. *IEEE Trans. Nanobioscience* **3,** 66–73 (2004).

59. Weissleder, R., Bogdanov, A., Neuwelt, E. A. & Papisov, M. Long-circulating iron oxides for MR imaging. *Advanced Drug Delivery Reviews* **16,** 321–334 (1995).

60. Reimer, P. & Weissleder, R. Development and experimental use of receptor-specific MR contrast agents. *Radiologe* **36,** 153–163 (1996).

61. Chouly, C., Pouliquen, D., Lucet, I., Jeune, J. J. & Jallet, P. Development of superparamagnetic nanoparticles for MRI: effect of particle size, charge and surface nature on biodistribution. *J. Microencapsul.* **13,** 245–255 (1996).

62. Araújo, J. E. *et al.* Novel nanocomposites based on a strawberry-like gold- coated magnetite (Fe@Au) for protein separation in multiple myeloma serum samples. *Nano Res.* **8,** 1189–1198 (2015).

63. Lu, A. H., Salabas, E. L. & Schuth, F. Magnetic nanoparticles: Synthesis, protection, functionalization, and application. *Angewandte Chemie - International Edition* **46,** 1222–1244 (2007).

64. Sadhukha, T., Wiedmann, T. S. & Panyam, J. Inhalable magnetic nanoparticles for targeted hyperthermia in lung cancer therapy. *Biomaterials* **34,** 5163–5171 (2013).

65. Conde, J. *et al.* Design of multifunctional gold nanoparticles for in vitro and in vivo gene silencing. *ACS Nano* **6,** 8316–8324 (2012).

66. Bao, C. *et al.* A promising road with challenges: where are gold nanoparticles in translational research? *Nanomedicine (Lond).* **9,** 2353–70 (2014).

67. Zhao, J., Bo, B., Yin, Y.-M. & Li, G.-X. Gold Nanoparticles-Based Biosensors for biomedical application. *Nano Life* **02,** 1230008 (2012).

68. Llevot, A. & Astruc, D. Applications of vectorized gold nanoparticles to the diagnosis and therapy of cancer. *Chem. Soc. Rev.* **41,** 242 (2012).

69. Silva, A. S. *et al.* Nanogold Poxylation: Towards always-on fluorescent lung cancer targeting. *RSC Adv.* **16,** 1–3 (2016).

70. Mero, A., Clementi, C., Veronese, F. M. & Pasut, G. Covalent conjugation of poly(ethylene glycol) to proteins and peptides: strategies and methods. *Methods Mol. Biol.* **751,** 95–129 (2011).

71. Mero, A. *et al.* Synthesis and characterization of poly(2-ethyl 2-oxazoline)-conjugates with proteins and drugs: Suitable alternatives to PEG-conjugates? *J. Control. Release* **125,** 87–95 (2008).

72. Correia, Vanessa G.; Bonifácio, Vasco D.B.; Raje, Vivek P.; Casimiro, Teresa; Moutinho, Guilhermina; Lobato da Silva, Cláudia; Pinho, Mariana G.; Aguiar-Ricardo, A. Oxazoline-Based Antimicrobial Oligomers: Synthesis by CROP Using Supercritical CO2. *Macromol. Biosci.* **11,** 1128–1137 (2011).

73. A. Aguiar-Ricardo, V.D.B. Bonifacio, T. Casimiro, V. G. C. Supercritical carbon dioxide design strategies: from drug carriers to soft killers. *Phil. Trans. R. Soc. A* **A 373.2057,** 20150009 (2015).

74. de Macedo, C. V., da Silva, M. S., Casimiro, T., Cabrita, E. J. & Aguiar-Ricardo, A. Boron trifluoride catalyzed polymerisation of 2-substituted-2-oxazolines in supercritical carbon dioxide. *Green Chem.* **9,** 948–953 (2007).

75. Restani, R. B. *et al.* POxylated Polyurea Dendrimers: Smart Core-Shell Vectors with IC50 Lowering Capacity. *Macromol. Biosci.* **15,** 1045–1051 (2015).

76. Dash, M., Chiellini, F., Ottenbrite, R. M. & Chiellini, E. Chitosan - A versatile semi-synthetic polymer in biomedical applications. *Prog. Polym. Sci.* **36,** 981–1014 (2011).

77. Temtem, M., Barroso, T., Casimiro, T., Mano, J. F. & Aguiar-Ricardo, A. Dual stimuli responsive poly(N-isopropylacrylamide) coated chitosan scaffolds for controlled release prepared from a non residue technology. *J. Supercrit. Fluids* **66,** 398–404 (2012).

78. Jae, H. P. *et al.* Self-assembled nanoparticles based on glycol chitosan bearing hydrophobic moieties as carriers for doxorubicin: In vivo biodistribution and anti-tumor activity. *Biomaterials* **27,** 119–126 (2006).

79. Kumirska, J., Czerwicka, M., Kaczyński, Z. & Bychowska, A. Application of Spectroscopic Methods for Structural Analysis of Chitin and Chitosan. *Mar. Drugs* **8,** 1567–1636 (2010).

80. Maya, S. *et al.* Chitosan cross-linked docetaxel loaded EGF receptor targeted nanoparticles for lung cancer cells. *Int. J. Biol. Macromol.* **69,** 532–541 (2014).

81. Kean, T. & Thanou, M. Biodegradation, biodistribution and toxicity of chitosan. *Advanced Drug Delivery Reviews* **62,** 3–11 (2010).

82. Peniche, C., Arguelles-Monal, W., Peniche, H. & Acosta, N. Chitosan: An Attractive Biocompatible Polymer for Microencapsulation. *Macromol. Biosci.* **3,** 511–520 (2003).

83. Lehr, C. M., Bouwstra, J. A., Schacht, E. H. & Junginger, H. E. In vitro evaluation of mucoadhesive properties of chitosan and some other natural polymers. *Int. J. Pharm.* **78,** 43–48 (1992).

84. Preparations for Inhalation: Aerodynamic Assessment of Fine Particles. *Eur. Pharmacop.* **Counc. Eur,** 274–285 (2010).

85. Roberts, D. L. & Mitchell, J. P. The effect of nonideal cascade impactor stage collection efficiency curves on the interpretation of the size of inhaler-generated aerosols. *AAPS PharmSciTech* **14,** 497–510 (2013).

86. Bosquillon, C., Lombry, C., Préaat, V. & Vanbever, R. Influence of formulation excipients and physical characteristics of inhalation dry powders on their aerosolization performance. *J. Control. Release* **70,** 329–339 (2001).

87. Shekunov, B. Y., Chattopadhyay, P., Tong, H. H. Y. & Chow, A. H. L. Particle size analysis in pharmaceutics: Principles, methods and applications. *Pharm. Res.* **24,** 203–227 (2007).

88. Ikegami, K. *et al.* A new agglomerated KSR-592 B-form crystal system for dry powder inhalation formulation to improve inhalation performance in vitro and in vivo. *J. Control.*

Release **88,** 23–33 (2003).

89. Greg, A. J. Adsorption, Surface Area and Porosity. *J. Catal.* **314,** 313–314 (1967).

90. Adsorption by Active Carbons. *Structure* (2000).

91. Arifin, D. Y., Lee, L. Y. & Wang, C. H. Mathematical modeling and simulation of drug release from microspheres: Implications to drug delivery systems. *Adv. Drug Deliv. Rev.* **58,** 1274–1325 (2006).

92. Peppas, N. A. & Sahlin, J. J. A simple equation for the description of solute release. III. Coupling of diffusion and relaxation. *Int. J. Pharm.* **57,** 169–172 (1989).

93. Ritger, P. L. & Peppas, N. A. simple equation for description of solute release I. Fickian and non-fickian release from non-swellable devices in the form of slabs, spheres, cylinders or discs. *J. Control. Release* **5,** 23–36 (1987).

94. Verges, M. A. *et al.* Uniform and water stable magnetite nanoparticles with diameters around the monodomain-multidomain limit. *J. Phys. D-Applied Phys.* **41,** 134003 (2008).

95. Turkevich, J., Garton, G. & Stevenson, P. C. The color of colloidal gold. *J. Colloid Sci.* **9,** 26–35 (1954).

96. Caruso, F., Lichtenfeld, H., Giersig, M. & Mohwald, H. Electrostatic self-assembly of silica nanoparticle-polyelectrolyte multilayers on polystyrene latex particles [4]. *J. Am. Chem. Soc.* **120,** 8523–8524 (1998).

97. Mayya, K. S., Schoeler, B. & Caruso, F. Preparation and organization of nanoscale polyelectrolyte- coated gold nanoparticles. *Adv. Funct. Mater.* **13,** 183–188 (2003).

98. Caruso, F., Susha, A. S., Giersig, M. & Möhwald, H. Magnetic Core-Shell Particles : Preparation of Magnetite Multilayers on Polymer Latex Microspheres. *Adv. Mater.* **11,** 950–953 (1999).

99. Mitchell, J. P. & Nagel, M. W. Cascade impactors for the size characterization of aerosols from medical inhalers: their uses and limitations. *J. Aerosol Med.* **16,** 341–377 (2003).

100. Korsmeyer, R. W., Gurny, R., Doelker, E., Buri, P. & Peppas, N. A. Mechanisms of solute release from porous hydrophilic polymers. *Int. J. Pharm.* **15,** 25–35 (1983).

101. Marianecci, Carlotta; Marzio, Luisa Di; Rinaldi, Frederica; Carafa, Maria; Alhaique, F. Pulmonary Delivery: Innovative Approaches and Perspectives. *J. Biomater. Nanobiotechnol.* **02,** 567–575 (2011).

102. Saquib Hasnain, M. & Nayak, A. K. Solubility and dissolution enhancement of ibuprofen by solid dispersion technique using peg 6000-PVP K 30 combination carrier. *Chemistry (Easton).* **21,** 118–132 (2012).

103. Mostaghim, S., Naderi, M. & Ghazitabar, A. Synthesis of magnetite–gold nanoshells by means of the secondary gold resource. *J. Iran. Chem. Soc.* **12,** 1709–1716 (2015).

104. Robinson, I., Tung, L. D., Maenosono, S., Wälti, C. & Thanh, N. T. K. Synthesis of core-shell gold coated magnetic nanoparticles and their interaction with thiolated DNA. *Nanoscale* **2,** 2624–2630 (2010).

105. Dolovich, M. B. & Dhand, R. Aerosol drug delivery: Developments in device design and clinical use. *Lancet* **377,** 1032–1045 (2011).

6

Appendix

6.1 Absorbances and Fluorescence Assays

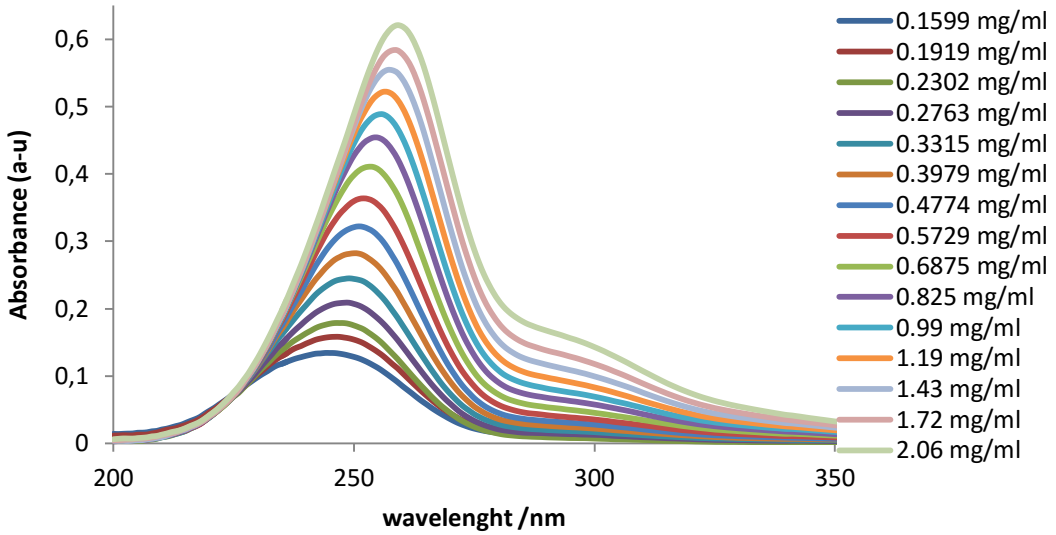

Figure A30 Absorbance at different concentrations of the polymer

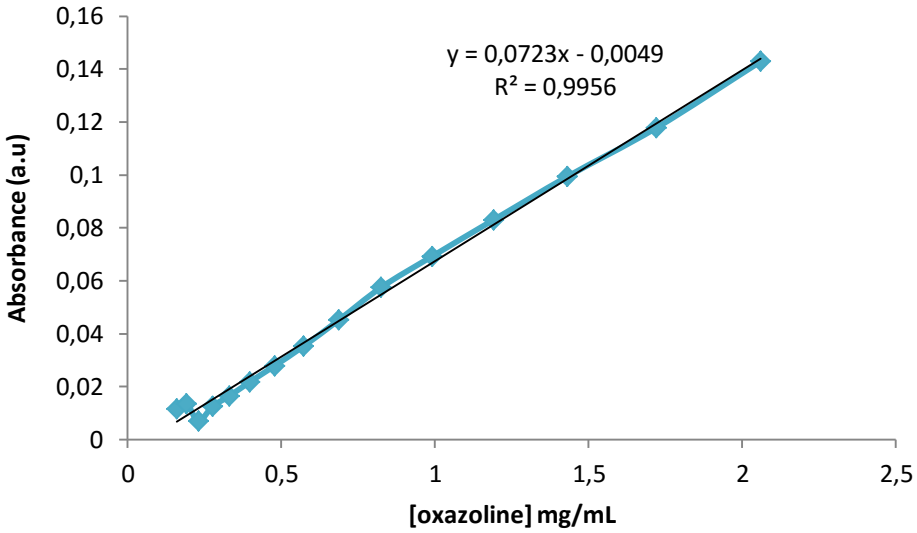

Figure A31 Calibration curve of the polymer

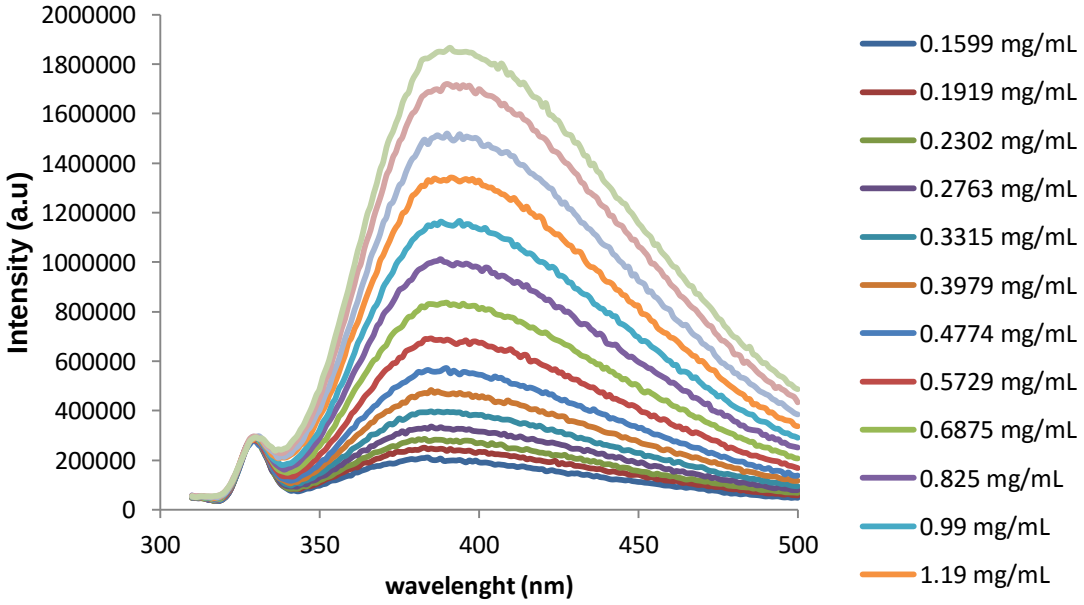

Figure A32 Polymer intensities at different concentrations

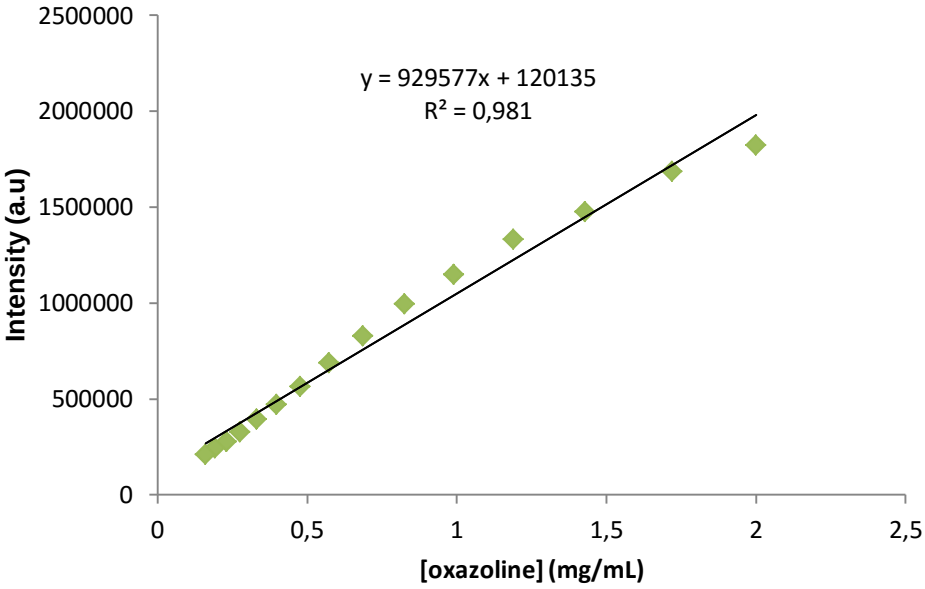

Figure A33 Calibration curve at different polymer concentrations

6.2 – NMR spectra of the oligo(2-ethyl-2-oxazoline): ^{1}H and ^{13}C

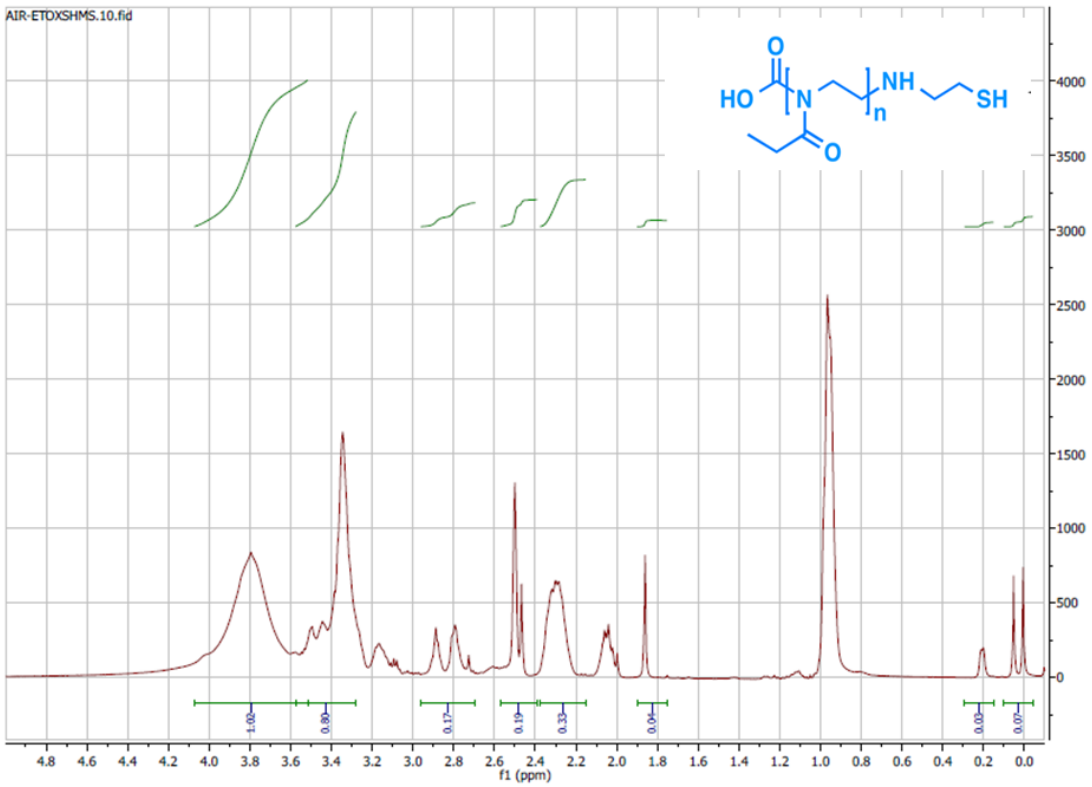

Figure A34 ^{1}H NMR spectrum of the polymer

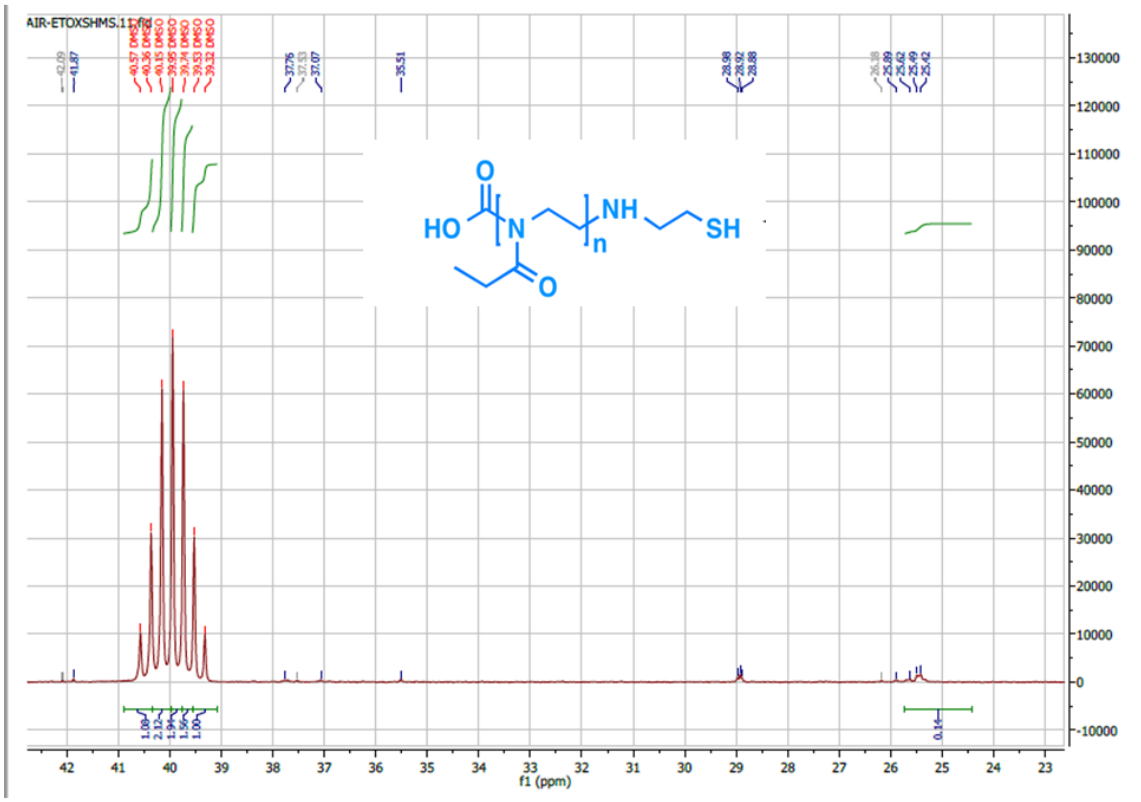

Figure A35 ^{13}C Spectrum of the polymer

6.3 – Drug release data

Table 14 Absorbances and concentrations of the drug release study at pH 6.4

pH 6.4	Absorbances				Absorbances corrected			Concentration			Average	In 5 mL		
	20.6 mg	20.9 mg	20.8 mg	20.5 mg										
t	CHT	IBP 1	IBP 2	IBP 3	IBP 1	IBP 2	IBP 3	IBP 1	IBP 2	IBP 3		IBP 1	IBP 2	IBP 3
0.25	0.186	0.81	0.752	0.427	0.624	0.566	0.241	0.030531	0.027694	0.011792	0.035130639	0.152657	0.138468	0.235835
0.5	0.179	0.306	0.243	0.601	0.127	0.064	0.422	0.006214	0.003131	0.020648	0.039990867	0.124278	0.062628	0.412956
0.75	0.175	0.346	0.446	0.521	0.171	0.271	0.346	0.008367	0.01326	0.016929	0.051407509	0.167335	0.265192	0.338585
0.017	0.176	0.494	0.434	0.577	0.318	0.258	0.401	0.015559	0.012624	0.01962	0.063737482	0.311185	0.252471	0.392406
1.5	0.154	0.521	0.512	0.692	0.367	0.358	0.538	0.017957	0.017516	0.026324	0.082395538	0.359135	0.350328	0.52647
2	0.136	0.586	0.588	0.695	0.45	0.452	0.559	0.022018	0.022116	0.027351	0.095312653	0.440356	0.442313	0.54702
2.5	0.187	0.597	0.623	0.671	0.41	0.436	0.484	0.020061	0.021333	0.023681	0.086766481	0.401213	0.426656	0.473628
3	0.107	0.529	0.576	0.649	0.422	0.469	0.542	0.020648	0.022947	0.026519	0.09348599	0.412956	0.458949	0.530385
3.5	0.094	0.521	0.587	0.572	0.427	0.493	0.478	0.020892	0.024122	0.023388	0.091202662	0.417849	0.482435	0.467756
4	0.096	0.614	0.68	0.586	0.518	0.584	0.49	0.025345	0.028574	0.023975	0.103858825	0.506899	0.571484	0.479499
5	0.091	0.581	0.643	0.515	0.49	0.552	0.424	0.023975	0.027009	0.020746	0.095638843	0.479499	0.54017	0.414913
6	0.111	0.465	0.545	0.429	0.354	0.434	0.318	0.017321	0.021235	0.015559	0.072153179	0.346414	0.424699	0.311185
7	0.085	0.478	0.475	0.363	0.393	0.39	0.278	0.019229	0.019082	0.013602	0.069217471	0.384578	0.381642	0.272042
8	0.099	0.369	0.424	0.305	0.27	0.325	0.206	0.013211	0.015902	0.010079	0.052255602	0.264214	0.318035	0.201585
9	0.132	0.368	0.382	0.209	0.236	0.25	0.077	0.011547	0.012232	0.003767	0.036728969	0.230942	0.244642	0.07535
24	0.21	0.348	0.378	0.215	0.138	0.168	0.005	0.006752	0.00822	0.000245	0.020289004	0.135043	0.1644	0.004893
48	0.367	0.395	0.39	0.371	0.028	0.023	0.004	0.00137	0.001125	0.000196	0.003588088	0.0274	0.022507	0.003914

Table 15 Aborbances and concentrations of the drug relase study at pH 7.4

pH 7.4	Absorbances				Aborbances correctes			Concentration			Average	In 5 mL		
	20.9 mg	21 mg	20.4 mg	21.2 mg										
t	CHT	IBP 3	IBP 4	IBP 5	IBP 3	IBP 4	IBP 5	IBP 3	IBP 4	IBP 5		IBP 3	IBP 4	IBP 5
0.25	0.166	0.863	0.681	0.338	0.697	0.515	0.172	0.034103	0.025198	0.008416	0.030988	0.170516	0.125991	0.168314
0.5	0.172	0.302	0.585	0.282	0.13	0.413	0.11	0.006361	0.020207	0.005382	0.027009	0.095411	0.202075	0.107643
0.75	0.163	0.247	0.731	0.347	0.084	0.568	0.184	0.00411	0.027791	0.009003	0.034641	0.06165	0.277914	0.180057
0.017	0.13	0.277	0.972	0.471	0.147	0.842	0.341	0.007192	0.041198	0.016685	0.056904	0.107887	0.411978	0.333692
1.5	0.148	0.591	0.524	0.475	0.443	0.376	0.327	0.021675	0.018397	0.016	0.067538	0.32513	0.367942	0.319992
2	0.144	0.562	0.608	0.499	0.418	0.464	0.355	0.020452	0.022703	0.01737	0.073882	0.306781	0.454056	0.347392
2.5	0.119	0.588	0.577	0.478	0.469	0.458	0.359	0.022947	0.022409	0.017565	0.076247	0.344212	0.448185	0.351306
3	0.103	0.609	0.535	0.451	0.506	0.432	0.348	0.024758	0.021137	0.017027	0.075643	0.371367	0.422742	0.340542
3.5	0.096	0.575	0.474	0.399	0.479	0.378	0.303	0.023437	0.018495	0.014825	0.067864	0.351551	0.369899	0.296507
4	0.111	0.624	0.553	0.467	0.513	0.442	0.356	0.0251	0.021626	0.017419	0.07716	0.376505	0.432528	0.348371
5	0.127	0.666	0.586	0.484	0.539	0.459	0.357	0.026372	0.022458	0.017467	0.079607	0.395587	0.449163	0.349349
6	0.132	0.628	0.527	0.425	0.496	0.395	0.293	0.024269	0.019327	0.014336	0.069152	0.364028	0.386535	0.286721
7	0.144	0.586	0.458	0.396	0.442	0.314	0.252	0.021626	0.015364	0.01233	0.058551	0.324396	0.307271	0.246599
8	0.177	0.486	0.436	0.388	0.309	0.259	0.211	0.015119	0.012672	0.010324	0.045781	0.226783	0.253449	0.206478
9	0.168	0.491	0.366	0.35	0.323	0.198	0.182	0.015804	0.009688	0.008905	0.040594	0.237058	0.193757	0.1781
24	0.38	0.644	0.425	0.423	0.264	0.045	0.043	0.012917	0.002202	0.002104	0.018658	0.193757	0.044036	0.042078
48	0.35	0.439	0.427	0.439	0.089	0.077	0.089	0.004355	0.003767	0.004355	0.016636	0.087093	0.07535	0.087093